ELSEVIER

Soil Dynamics and Earthquake Engineering 26 (2006) 824–853

SOIL DYNAMICS AND EARTHQUAKE ENGINEERING

www.elsevier.com/locate/soildyn

Footings under seismic loading: Analysis and design issues with emphasis on bridge foundations

George Mylonakis[a,*], Sissy Nikolaou[b], George Gazetas[c]

[a]*University of Patras, Rio GR-26500, Greece*
[b]*Mueser Rutledge Consulting Engineers, USA*
[c]*National Technical University, Athens, Greece*

Accepted 9 December 2005

Abstract

The paper provides state-of-the-art information on the following aspects of seismic analysis and design of spread footings supporting bridge piers: (1) obtaining the dynamic stiffness ("springs" and "dashpots") of the foundation; (2) computing the kinematic response; (3) determining the conditions under which foundation–soil compliance must be incorporated in dynamic structural analysis; (4) assessing the importance of properly modeling the effect of embedment; (5) elucidating the conditions under which the effect of radiation damping is significant; (6) comparing the relative importance between kinematic and inertial response. The paper compiles an extensive set of graphs and tables for stiffness and damping in all modes of vibration (swaying, rocking, torsion), for a variety of soil conditions and foundation geometries. Simplified expressions for computing kinematic response (both in translation and rotation) are provided. Special issues such as presence of rock at shallow depths, the contribution of foundation sidewalls, soil inhomogeneity and inelasticity, are also discussed. The paper concludes with parametric studies on the seismic response of bridge bents on embedded footings in layered soil. Results are presented (in frequency and time domains) for accelerations and displacements of bridge and footing, while potential errors from some frequently employed simplifications are illustrated.
© 2006 Elsevier Ltd. All rights reserved.

Keywords: Dynamics; Footings; Impedance; Kinematic response; Soil–structure interaction; Numerical methods

1. Introduction

During earthquake shaking, soil deforms under the influence of the incident seismic waves and "carries" dynamically with it the foundation and the supported structure. In turn, the induced motion of the superstructure generates inertial forces which result in dynamic stresses at the foundation that are transmitted into the supporting soil. Thus, superstructure-induced deformations develop in the soil while additional waves emanate from the soil–foundation interface. In response, foundation and superstructure undergo further dynamic displacements, which generate further inertial forces and so on.

The above phenomena occur simultaneously. However, it is convenient (both conceptually and computationally) to separate them into two successive phenomena referred to as "kinematic interaction" and "inertial interaction" [1–4], and obtain the response of the soil–foundation–structure system as a superposition of these two interaction effects:

(a) "Kinematic interaction" (KI) refers to the effects of the incident seismic waves to the system shown in Fig. 1b, which consists essentially of the foundation and the supporting soil, with the mass of the superstructure set equal to zero (in contrast to the complete system of Fig. 1a). The main consequence of KI is that it leads to a "foundation input motion" (FIM) which is different (usually smaller) than the motion of the free-field soil and, in addition, contains a rotational component. As will be shown later on, this difference could be significant for embedded foundations.

(b) "Inertial interaction" (II) refers to the response of the complete soil–foundation–structure system to the

*Corresponding author.
E-mail address: mylo@upatras.gr (G. Mylonakis).

0267-7261/$ - see front matter © 2006 Elsevier Ltd. All rights reserved.
doi:10.1016/j.soildyn.2005.12.005

Nomenclature

$a_k(t)$	kinematic acceleration
$\mathscr{A}$	soil surface-to-rock motion amplification function
A_b	foundation basemat–soil contact area
A_w	total area of actual sidewall–soil contact surface
A_{wce}	sum of projections of total sidewall area in direction perpendicular to loading
A_{ws}	sum of projections of total sidewall area in direction parallel to loading
b	soil inhomogeneity parameter
B	foundation halfwidth or "equivalent" radius in the direction examined, or of circumscribed rectangle
C, C_z, C_y, C_{ij}	dashpot coefficient
C_{rad}	radiation damping coefficient
d	total height of actual sidewall–soil contact surface
d_c	diameter of bridge pier
D	depth of embedment
E_s	soil modulus of elasticity
E_c	concrete modulus of elasticity
f	frequency
f_c	fundamental natural frequency of soil deposit in compression–extension
f_D	natural frequency in shear mode of a hypothetical soil stratum of thickness D
f_s	fundamental natural frequency of soil deposit in shear mode
$F(U_A)$	Fourier amplitude spectrum of design motion at free-field soil surface
FS	factor of safety
g	acceleration of gravity
G, G_0	soil shear modulus, maximum (low-strain) soil shear modulus
G_0, G_∞	soil shear modulus at zero and infinite depth, respectively
h	distance of (effective) sidewall centroid from ground surface
H	soil thickness
H_c	height of bridge pier
H_ε	horizontal force amplitude due to inertia on the masses of the superstructure
i	$\sqrt{-1}$
I_1	mass moment of inertia of bridge superstructure
I_b	polar moment of inertia about z of soil foundation contact surface
I_{bx}	moment of inertia about x of soil foundation contact surface
I_{by}	moment of inertia about y of soil foundation contact surface
I_Φ	rotational kinematic interaction factors
I_0	mass moment of inertia of bridge foundation
I_R	impedance contrast between soil and rock
I_U	translational kinematic interaction factors
k	wavenumber
K	static stiffness
$\bar{K}$, $\bar{K}_z$	dynamic stiffness ("spring")
k, $k(\omega)$	dynamic stiffness coefficient
$\bar{K}_{sur}$, C_{sur}	dynamic stiffness and dashpot coefficients of surface foundation
K_{emb}, C_{emb}	dynamic stiffnesses and dashpot coefficients of embedded foundation
$\mathscr{K}_x$	swaying foundation impedance
$\mathscr{K}_y$	swaying impedance in long direction
$\mathscr{K}_{rx}$	rocking impedance about long axis of foundation basemat
$\mathscr{K}_{ry}$	rocking impedance about short axis of foundation basemat
$\mathscr{K}_t$	torsional impedance about vertical axis
$\mathscr{K}_{x-ry}$, $\mathscr{K}_{y-rx}$	cross-coupling horizontal-rocking impedances
$\mathscr{K}_{str}$	dynamic structural impedance of superstructure
L	semi-length of footing (or of circumscribed rectangle)
m_1, m_s	superstructure mass
M_ε	overturning moment amplitude due to inertia on the masses of the superstructure
m_0, m_b	foundation mass
n	soil inhomogeneity parameter
P	axial gravity load carried by bridge system
PGA	peak ground acceleration
P_z, P_z(t)	vertical force
q, q_u	applied foundation pressure
R	radius of bridge footing
SA	spectral acceleration
S_u	soil undrained shear strength
t	time
T, $\tilde{T}$	period, effective period
$u_z(t)$, u_1, u_2	vertical foundation displacement
U_A, U_G	motions at depths A and G, respectively
V_a	apparent wave propagation velocity along ground surface or soil–foundation interface
V_{La}, V_{Lao}	"Lysmer's analog" wave velocity, "Lysmer's analog" wave velocity at surface
V_r	shear wave velocity of rock
V_R	Rayleigh wave velocity
V_s, V_{so}	soil shear wave velocity, soil shear wave velocity at surface
z	depth
z_r	depth of influence
z_v, z_h, z_r, z_t	depths of influence in vertical, horizontal, rocking, and torsional vibrations

Greek letters

α, ϕ	phase angle (α also Ramber-Osgood parameter)

β, β_{ij}	linear hysteretic damping factors	ρ_s	soil mass density
γ	soil unit weight	σ_z	vertical normal stress
γ_c	cyclic shear strain amplitude in percent	τ, τ_c	soil shear stress
γ_y	characteristic shear strain	Φ	free-field rotation
λ_R	Rayleigh wave length	Φ_0	foundation rotation
ν	Poisson's ratio	Φ_G	rotation about out-of-plane horizontal axis through foundation center
ξ, $\tilde{\xi}$	damping, effective damping of soil-structure system	ψ	angle of incidence of S wave along the horizontal axis
Ξ_0	inhomogeneity parameter		
ρ_r	elastic rock mass density	ω	cyclic frequency

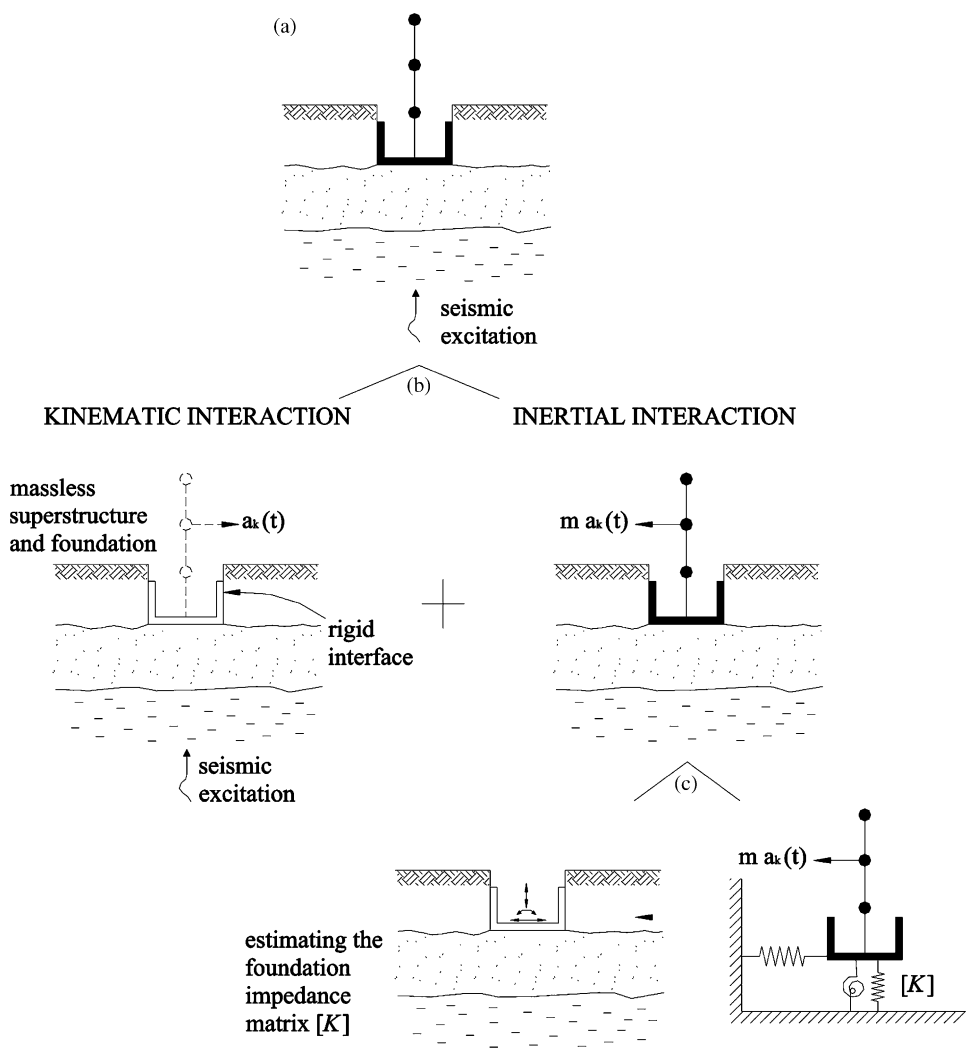

Fig. 1. (a) The geometry of soil–structure interaction problem; (b) decomposition into kinematic and inertial response; (c) two-step analysis of inertial interaction (modified after Kausel et al. [5]).

excitation by D'Alembert forces associated with the acceleration of the superstructure due to the KI (Fig. 1b).

Furthermore, for a surface or embedded foundation, II analysis is also conveniently performed in two steps, as shown in Fig. 1c: first compute the foundation dynamic impedance ("springs" and "dashpots") associated with each mode of vibration, and then determine the seismic response of the structure and foundation supported on these springs and dashpots, and subjected to the kinematic accelerations $a_k(t)$ of the base. The following section presents methods and results for each of these steps.

2. Assessing the effects of kinematic interaction

The first step of the KI analysis is to determine the free-field response of the site, that is, the spatial and temporal

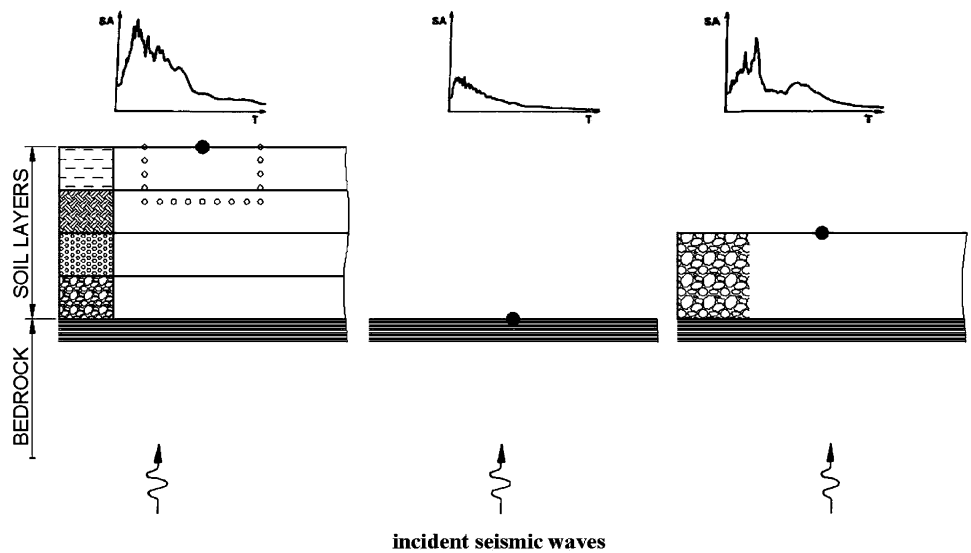

Fig. 2. Selection of "control" point where seismic excitation is specified.

variation of the ground motion before building the structure. This task requires that:

(a) The *design motion* be known at a specific ("*control*") point, which is usually taken at the ground surface or at the rock-outcrop surface, as shown in Fig. 2. Most frequently the design motion is given in the form of a *design response spectrum* in the horizontal direction and sometimes also in the vertical direction.

(b) The type of seismic waves that produce the above motion at the "control" point may be either estimated from a site-specific seismological study based on available data, or simply assumed in an engineering manner. In most cases the assumption is that the horizontal component of motion is due solely to either vertically propagating shear (S) waves or vertical dilatational (P) waves. In critical projects other wave patterns (e.g., oblique body waves, surface waves) may have to be considered.

Having established (a) and (b), wave-propagation analyses are performed to estimate the free-field motion along the soil–foundation interface. The equivalent linear computer code SHAKE [6] is a well established tool for performing such analyses, and can be used for any possible location of the control point (at the ground surface, at the rock outcrop surface, or the base of the soil deposit). Other codes, performing truly nonlinear response analyses (DESRA, DYNAFLOW, CHARSOIL, STEALTH, ANDRES, WAVES, etc.) require that the base motion be first estimated and used as input. In these techniques, the "control" point should be at the base of the profile.

2.1. Simplified site response analysis

For the case of SH or SV harmonic waves propagating vertically through the soil with frequency ω, the variation of motion with depth in the free field of a horizontally stratified deposit will be given by one-dimensional amplification theory. For a homogeneous soil layer, the amplitude of the motion at any depth z, U_G, relates to the motion at the ground surface, U_A, as follows [1,7]:

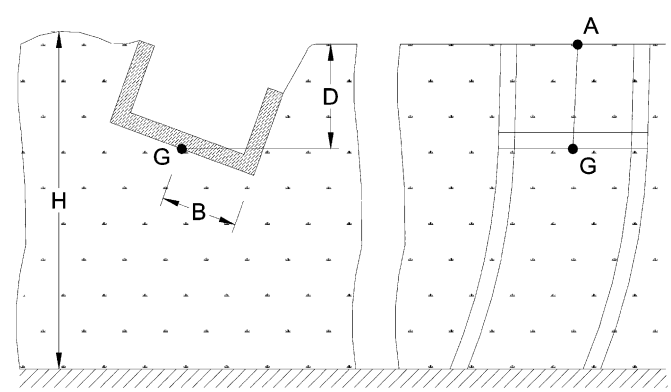

Fig. 3. Definition of points A and G in the free field with reference to kinematic response of a massless foundation (from [8]).

$$\mathscr{A} \equiv \frac{U_G}{U_A} = \cos(\mathscr{k} z), \tag{1}$$

where $\mathscr{k}$ = a complex "wavenumber" in view of the presence of material damping in the soil given by

$$\mathscr{k} = \frac{\omega}{V_s\sqrt{1+2i\beta}}, \tag{2}$$

where ω is the excitation frequency, V_s the propagation velocity of shear waves in the soil, $i = \sqrt{-1}$, β the linear hysteretic damping coefficent of soil material.

If material damping is ignored, function $\mathscr{A}$ simplifies to

$$\mathscr{A} = \cos(\omega z / V_s). \tag{3}$$

For any bearing specific depth $z = D$ (see also Fig. 3), this transfer function becomes zero whenever $\omega = (2n+1)(\pi/2)(V_s/D)$, which are the natural frequencies in

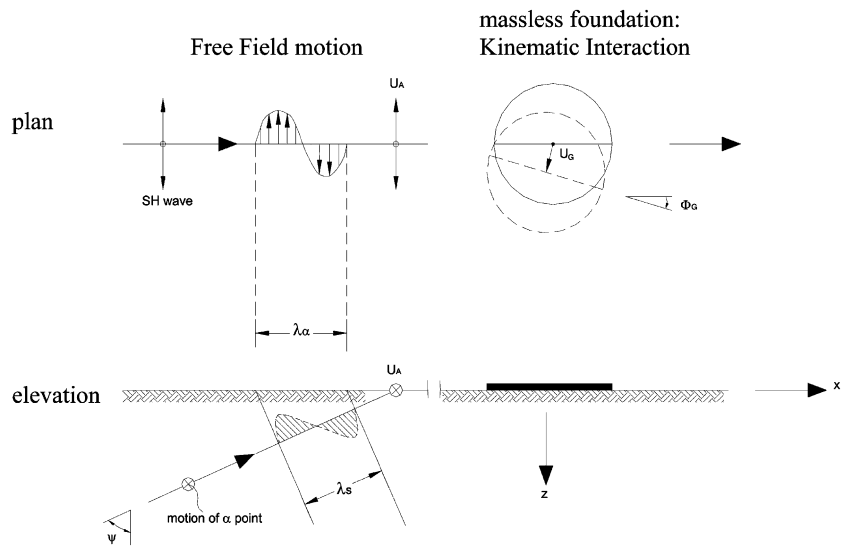

Fig. 4. Inclined SH wave, apparent wave length ($\lambda_\alpha = \lambda_s/\sin\psi$), free-field surface motion (U_A), and foundation effective input motion (U_G,Φ_G).

shear vibrations of a stratum of thickness D. This implies that these frequencies would be entirely filtered out from the seismic motion at the foundation depth D.

Since the transfer function in Eq. (1) is equal to or less than 1 over the whole frequency range, the motion will always be de-amplified with depth. This is no longer true if internal damping exists in the soil, but for moderate values of damping the transfer function will still show some important variations with frequency and the motion at the depth D will still be less than at the surface.

It is also possible in the free field to define a rotation function (Fig. 3):

$$\Phi = \frac{U_A - U_G}{D}, \tag{4}$$

which pertains to a perfectly flexible embedded foundation subjected to a vertically propagating seismic wavefield. In more ridid foundations, the rotation would tend to be less than the above estimate. Accordingly, Φ can be treated as an upper-bound of the actual foundation rotation. Also, for a surface foundation subjected to a traveling seismic wave, points A and G should be taken at the same elevation. The rocking and torsional response of the foundation induced by such an excitation will be influenced by the destructive interference of the incoming waves—the so-called "tau effect" of Newmark [9]. Only the former case is discussed in this work.

For a homogeneous stratum with zero internal damping, the rotation in Eq. (4) becomes

$$\Phi = \frac{U_A}{D}\left[1 - \cos\left(\frac{\omega D}{V_s}\right)\right] = 2\frac{U_A}{D}\sin^2\left(\frac{\omega D}{V_s}\right). \tag{5}$$

2.2. Simplified kinematic interaction analysis: foundation input motion

The displacement and rocking rotation in Eqs. (1) and (5) refer to depth D in the free field and constitute the driving motion for the kinematic response of the foundation. The presence of a more-or-less rigid embedded foundation *diffracts* the 1-D seismic waves, since its rigid body motion is generally incompatible with the free-field motion. The wave field now becomes much more complicated and the resulting motion of the foundation differs from the free-field motion, and includes a translational and a rotational component. Since, according to Fig. 1, this foundation motion is used as *excitation* in the II step of the whole seismic response analysis, it is termed FIM.

The following simple expressions (based on results by Luco [10], Elsabee et al. [11], Tassoulas [12], Harada et al. [13], Wolf [14]) can be used for estimating the translational and rocking components of FIM in some characteristic cases. Specifically:

(a) For a surface foundation subjected to vertically propagating S waves:

$$U_G \approx U_A, \tag{6}$$

$$\Phi_G \approx 0, \tag{7}$$

where Φ_G is the rocking component of the motion. Eqs. (6) and (7) imply that there is no kinematic effect, and that the FIM includes only a translation equal to the free-field ground surface motion.

(b) For a surface foundation subjected to oblique S or surface (Rayleigh or Love) waves, one must first determine the apparent propagation velocity V_α along the horizontal x axis (Fig. 4). Calling ψ the angle of incidence

of an S wave:

$$V_a = \frac{V_s}{\sin\psi}. \tag{8}$$

Different choices for the value of ψ can be made and the one leading to the largest structural response should be selected.

For surface waves, V_α will be determined from the dispersion relation of the soil deposit for each particular frequency ω. For Rayleigh waves in a practically homogeneous and deep soil deposit, V_α turns out to be only slightly less than V_s [15]. In this case, of course, Eq. (8) is inapplicable. For a deposit consisting of multiple layers of total thickness H having an average S-wave velocity V_s $(= H/\Sigma H_i/V_i)$ and underlain by a halfspace ("rock") of shear wave velocity V_r, V_α varies between V_s (lower limit at high frequencies) and $0.9 \times V_r$ (upper limit at low frequencies) as follows [16,17,63]:

$$V_a = \begin{cases} 0.90V_r, & f \leqslant f_H, \\ V_s, & f \geqslant 2f_H, \\ 0.90V_r - (0.90V_r - V_s) & \\ \times(f/f_H - 1), & f_H < f \leqslant 2f_H, \end{cases} \tag{9a–c}$$

where $f_H = V_s/4H$ is the fundamental natural frequency of the deposit.

Finally, for a deposit with stiffness increasing continuously with depth, V_α is only slightly less than the S-wave velocity V_s (z_c) at a depth [16,18]

$$z_c \approx \tfrac{1}{3}\lambda_R, \tag{10a}$$

where $\lambda_R = V_R/f$ is the wave length of the Rayleigh wave.

Apart from the above theoretical considerations, numerous indirect measurements of the apparent phase wave velocity of body waves along the ground surface have been reported in the literature (e.g., [17]). A key conclusion from these measurements is that the apparent velocity, even in soft soils (characterized by S-wave velocity of the order of 150 m/s), attains values in excess of

$$V_a = 1500\ \text{m/s}. \tag{10b}$$

This is an indirect evidence of the dominance of near-vertical S waves. Seismic codes for bridges (e.g. EC8/Part2-Bridges) have began to recognize these high values of phase velocity.

Note that the above equations have been derived for free-field conditions; their applicability to footings has not been rigorously tested. Gazetas [16] first studied the problem of equivalent depth for some profiles. Vrettos [18] derived the exact solution for exponential variation of soil modulus with depth, for a wide range of frequencies and soil profile parameters. Another interesting work on equivalent depth for SH-surface waves is given in Ref. [19]. For this type of wave, the equivalent depth is approximately 0.2 λ.

Once the apparent velocity V_α along the horizontal x-axis is estimated, the components of FIM can be determined from the following relations (based on the works of Luco and Westman [20], Elsabee et al. [8], Tassoulas [21], and Harada et al. [22]):

- Horizontal translation:

$$U_G = U_A \times I_U(\omega) \tag{11a}$$

$$I_U(\omega) = \frac{\sin(\omega B/V_\alpha)}{\omega B/V_\alpha}, \quad \frac{\omega B}{V_\alpha} \leqslant \frac{\pi}{2}, \tag{11b}$$

$$= \frac{2}{\pi}, \quad \frac{\omega B}{V_\alpha} > \frac{\pi}{2}. \tag{11c}$$

- Rocking rotation:

$$\Phi_G = \frac{U_A}{B} \times I_\Phi(\omega), \tag{12a}$$

where

$$I_\Phi = 0.30\left[1 - \cos\left(\frac{\omega B}{V_\alpha}\right)\right], \quad \frac{\omega B}{V_\alpha} \leqslant \frac{\pi}{2}, \tag{12b}$$

$$= 0.30, \quad \frac{\omega B}{V_\alpha} > \frac{\pi}{2}, \tag{12c}$$

in which B is the foundation halfwidth or "equivalent" radius in the direction examined; ω the cyclic frequency of harmonic seismic waves; Φ_G denotes the rocking rotation about the out-of-plane horizontal axis through the foundation center.

(c) For a foundation *embedded* at depth D and subjected to vertical and oblique SH waves, the horizontal and rotational component of FIM are approximately [8,20–22]:

$$U_G = U_A \times I_U(\omega), \tag{13a}$$

$$I_U(\omega) = \cos\left(\frac{\pi}{2}\frac{f}{f_D}\right), \quad f \leqslant \frac{2}{3}f_D, \tag{13b}$$

$$= 0.50, \quad f \geqslant \frac{2}{3}f_D, \tag{13c}$$

$$\Phi_G = \frac{U_A}{B} \times I_\Phi(\omega), \tag{14a}$$

$$I_\Phi(\omega) = 0.20\left[1 - \cos\left(\frac{\pi}{2}\frac{f}{f_D}\right)\right], \quad f \leqslant f_D, \tag{14b}$$

$$= 0.20, \quad f \geqslant f_D, \tag{14c}$$

in which $f = \omega/2\pi$ is the frequency in Hz of the harmonic seismic wave; $f_D = V_s/4D$ the frequency in shearing oscillations of a hypothetical soil stratum of thickness D. As a first approximation, Eqs. (13)–(17) apply to all foundation geometries.

Note that the rotation is an integral and important part of the base motion of the massless foundation. Ignoring it, while de-amplifying the translational component through the transfer function $I_U(\omega)$, may lead to errors on the

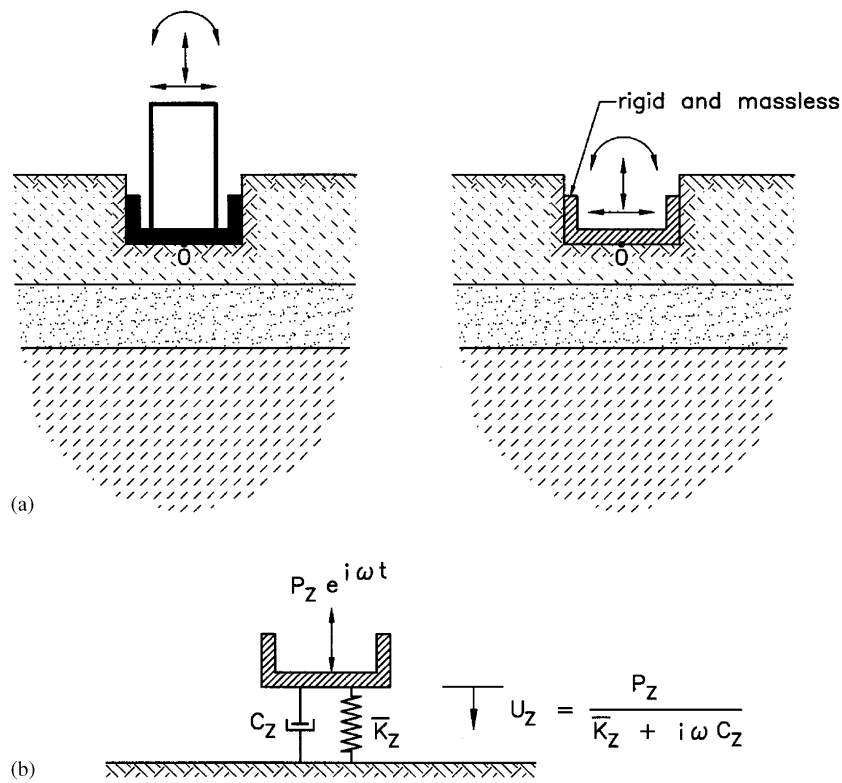

Fig. 5. Physical interpretation of dynamic spring and dashpot in vertical mode of vibration.

unsafe side. These errors are perhaps negligible for determining the response of short squatty structures—especially very heavy ones, but may be substantial (of the order of 50% or more) for tall slender structures [23]. On the other hand, ignoring both the de-amplification of the horizontal component ($I_U = 1$) and the existence of the rotational component ($I_\Phi = 1$) usually leads to slightly conservative results; this is a simplification frequently followed in practice for noncritical structures [24].

2.3. Use of KI transfer functions

Eqs. (6)–(14) are transfer functions relating the free-field horizontal ground surface motion to the effective FIM in the frequency domain. The mathematically correct (but still approximate) way of using the functions is as follows:

- obtain the Fourier amplitude spectrum $F(U_A)$ of the design motion at the free-field ground surface,
- multiply $F(U_A)$ by $I_U(\omega)$ and by $I_\Phi(\omega)/B$ to obtain the Fourier amplitude spectra functions (U_G and Φ_G) of the components of the FIM,
- use these functions directly as excitation in the II analysis, if the latter is done,
- in the frequency domain, or obtain, through an inverse Fourier transformation, the corresponding time histories to be used as excitation in a time domain inertial response analysis.

In practice, the most frequently used method involves a further simplification. It makes use of *response spectra* rather than Fourier spectra, and is, therefore, particularly attractive whenever the design motion is specified in the form of a design spectrum, SA(ω) or PSA(ω), at the ground surface, which is the most usual case in design codes. The response spectrum of the *effective horizontal FIM* is approximated as the product of SA(ω) $\times I_U(\omega)$ for the acceleration to be applied at the foundation mass, and as the product SA(ω) $\times [I_U(\omega) + I_\Phi(\omega)H_c/B]$ for the acceleration to be applied at a structural mass located a vertical distance H_c from the base [25].

3. Inertial SSI: assessment of foundation "springs" and "dashpots"

As explained in Section 1, the first step in II analysis is to determine the foundation impedance corresponding to each mode of vibration. For the usual case of a rigid foundation, there are six modes of vibration: three translational (dynamic displacements along the axes x, y and z) and three rotational (dynamic rotations around the same axes).

For each mode, soil can be replaced for the dynamic analysis by a dynamic spring of stiffness $\bar{K}$ and by a dashpot of modulus C. Their values will be discussed later on. Fig. 5 illustrates the vertical spring and dashpot ($\bar{K}_z$ and C_z) of an embedded foundation. Subjected to harmonic vertical force $P_z(t) = P_z \cos(\omega t + a)$ with

amplitude P_z and frequency ω, this foundation experiences a harmonic steady-state displacement $u_z(t)$ which has the same frequency ω but is out-of-phase with P_z(t). Thus, $u_z(t)$ can be expressed in the following equivalent ways:

$$u_z(t) = u_z \cos(\omega t + a + \phi) = u_1 \cos(\omega t + a) + u_2 \sin(\omega t + a), \quad (15)$$

where the amplitude u_z and phase angle ϕ are related to the in-phase, u_1 and the 90°-out-of-phase, u_2, components according to

$$u_z = \sqrt{u_1^2 + u_2^2}, \quad (16a)$$

$$\tan\phi = \frac{u_2}{u_1}. \quad (16b)$$

We can rewrite the foregoing expressions in an equivalent and computationally beneficial way using complex notation:

$$P_z(\mathrm{t}) = \bar{P}_z \exp(\mathrm{i}\omega t), \quad (17a)$$

$$u_z(t) = \bar{u}_z \exp(\mathrm{i}\omega t), \quad (17b)$$

where now $\bar{P}_z$ and $\bar{u}_z$ are complex quantities

$$\bar{P}_z = P_{z1} + \mathrm{i}P_{z2}, \quad (18a)$$

$$\bar{u}_z = u_{z1} + \mathrm{i}u_{z2}. \quad (18b)$$

Eqs. (17) and (18) are equivalent to Eqs. (15) and (16) with the following relations being valid for the amplitudes:

$$P_z = |\bar{P}_z| = \sqrt{P_{z1}^2 + P_{z2}^2}, \quad (19a)$$

$$u_z = |\bar{u}_z| = \sqrt{u_{z1}^2 + u_{z2}^2}, \quad (19b)$$

while the two phase angles, α and ϕ, are included in the complex forms.

With P_z and u_z being out of phase or, alternatively, with $\bar{P}_z$ and $\bar{u}_z$ being complex numbers, the dynamic vertical impedance (force–displacement ratio) becomes:

$$\mathscr{K}_z = \frac{\bar{P}_z}{\bar{u}_z} = \bar{K}_z + \mathrm{i}\omega C_z, \quad (20)$$

in which both $\bar{K}_z$ and C_z are, in general, functions of frequency. The spring constant $\bar{K}_z$, termed *dynamic stiffness*, reflects the stiffness and inertia of the supporting soil; its dependence on frequency relates solely to the influence that frequency exerts on inertia, since soil material properties are to a good approximation frequency independent. The *dashpot coefficient* C_z reflects the two types of damping (radiation and material) generated in the system; the former due to energy carried by the waves spreading away from the foundation, and the latter due to energy dissipated in the soil through hysteretic action. As evident from Eq. (20), damping is responsible for the phase difference between the excitation P_z and the response u_z.

The definition in Eq. (20) is also applicable to each of the other five modes of vibration. Thus, we define as lateral (swaying) impedance $\mathscr{K}_y$ the ratio of the horizontal harmonic force over the resulting harmonic displacement $\bar{u}_y(t)$ in the same direction:

$$\mathscr{K}_y = \frac{\bar{P}_y}{\bar{u}_y} = \bar{K}_y + \mathrm{i}\omega C_y. \quad (21)$$

Similarly,

- $\mathscr{K}_y$ = the longitudinal (swaying) impedance (force–displacement ratio), for horizontal motion in the long direction,
- $\mathscr{K}_{\mathrm{r}x}$ = the rocking impedance (moment–rotation ratio), for rotational motion about the long axis of the foundation basemat,
- $\mathscr{K}_{\mathrm{r}y}$ = the rocking impedance (moment–rotation ratio), for rotational motion about the short axis of the foundation,
- $\mathscr{K}_{\mathrm{t}}$ = the torsional impedance (moment–rotation ratio), for rotational oscillation about the vertical axis.

Moreover, in embedded foundations and piles, horizontal forces along principal axes induce rotational in addition to translational oscillations; hence, a *cross-coupling* horizontal-rocking impedance also exists: $\mathscr{K}_{x-\mathrm{r}y}$ and $\mathscr{K}_{y-\mathrm{r}x}$. The coupling impedances are usually negligibly small in shallow foundations, but their effects may become appreciable for greater depths of embedment, owing to the moments about the base axes produced by horizontal soil reactions against the sidewalls.

3.1. Example: lateral seismic response of block foundation supporting a SDOF structure

We refer to Fig. 6 for an example on how to use the foundation "springs" and "dashpots" to determine the response of a complete structure to harmonic earthquake-type excitation. The foundation and structure possess two orthogonal axes of symmetry, x and y, and coupled horizontal (swaying) and rotational (rocking) oscillations take place. Of interest are the foundation horizontal displacement $U_0 \exp(\mathrm{i}\omega t)$ along the x-axis, foundation rotation $\Phi_0 \exp(\mathrm{i}\omega t)$ about the y-axis, and relative displacement of the structure $U_1 \exp(\mathrm{i}\omega t)$. The seismic excitation is given by the free-field surface displacement $U_A \exp(\mathrm{i}\omega t)$ of amplitude U_A and frequency ω.

As a first step, we determine the FIM, from the KI analysis. Using the information presented earlier,

$$U_{\mathrm{G}} = U_{\mathrm{A}} I_U(\omega) \quad \text{and} \quad \Phi_{\mathrm{G}} = U_{\mathrm{A}} I_U(\omega)/B,$$

where I_U and I_Φ are the appropriate KI factors for each frequency ω.

The governing D'Alembert equations for dynamic equilibrium of the foundation block and the structure are [26]:

$$\mathscr{K}_x(U_0 - U_{\mathrm{G}}) + \mathscr{K}_{x-\mathrm{r}y}(\Phi_0 - \Phi_{\mathrm{G}}) = \omega^2[m_0 U_0 + m_1(U_0 + H_{\mathrm{c}}\Phi_0 + U_1)], \quad (22a)$$

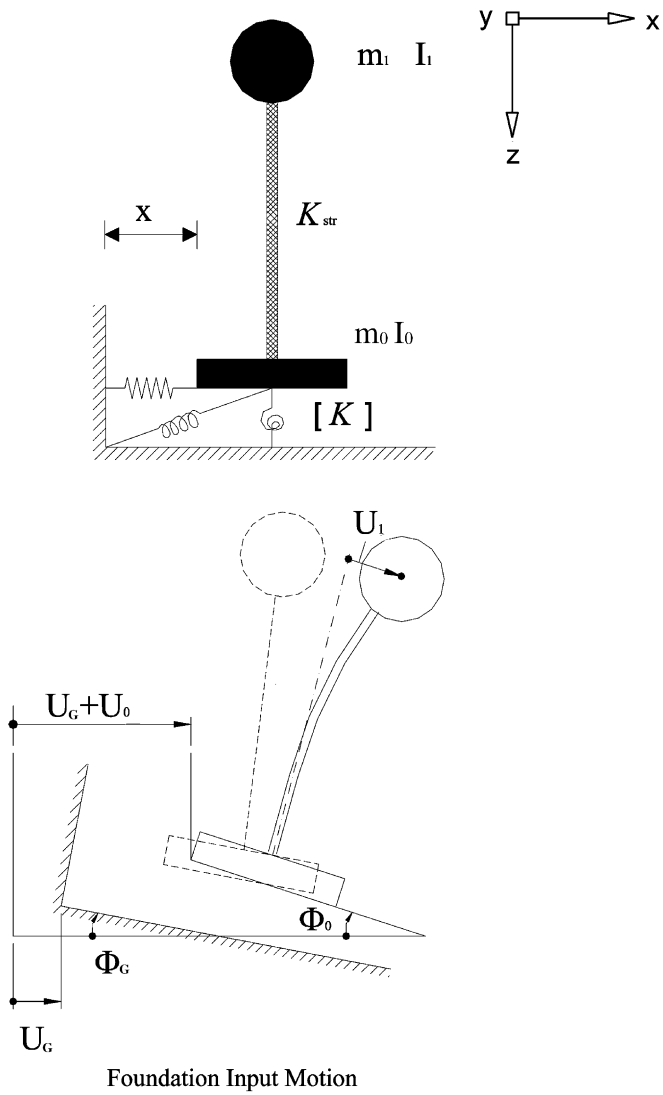

Fig. 6. Seismic displacements and rotation of a foundation block supporting a SDOF super-structure. The seismic excitation is described through the free-field ground-surface displacement U_A, assumed to be produced by a certain type of body or surface waves.

$$\mathscr{K}_{x-\mathrm{ry}}(U_0 - U_G) + \mathscr{K}_{\mathrm{ry}}(\Phi_0 - \Phi_G) = \omega^2[I_0\Phi_0 + I_1\Phi_0 + m_1 H_c(U_0 + H\Phi_0 + U_1)], \tag{22b}$$

$$-m_1\omega^2(U_0 + H_c\Phi_0 + U_1) + \mathscr{K}_{\mathrm{str}}U_1 = 0, \tag{22c}$$

in which m_0 and I_0 are the mass and mass moment of inertia of the foundation, m_1 and I_1 are the mass and mass moment of inertia of the superstructure and $\mathscr{K}_{\mathrm{str}} = K_{\mathrm{str}} + \mathrm{i}\omega C_{\mathrm{str}}$ the structural impedance (stiffness and damping) of the superstructure. Note that $\mathscr{K}_{x-\mathrm{ry}}$ is of minor importance in surface foundations, and is usually ommitted.[1] In embedded foundations, however, the term should be included, as it may have a profound influence in the response [27].

[1]This holds when the reference system is placed atop the footing ($z = 0$), as is usually the case.

The above equations define a simple algebraic system of three equations in three unknowns, despite the fact that the quantities involved are complex numbers. The solution, in matrix form, for the foundation motion is

$$\begin{Bmatrix} U_0 \\ \Phi_0 \end{Bmatrix} = \frac{K}{K - \omega^2(M_0 - M_b)} \begin{Bmatrix} U_G \\ \Phi_G \end{Bmatrix}, \tag{23a}$$

where

$$K = \begin{bmatrix} \mathscr{K}_x \mathscr{K}_{x-\mathrm{ry}} \\ \mathscr{K}_{\mathrm{ry}-x}\mathscr{K}_{\mathrm{ry}} \end{bmatrix}, \tag{23b}$$

$$[M_0] = \begin{bmatrix} m_0 & 0 \\ 0 & I_0 \end{bmatrix}, \tag{23c}$$

$$[M_b] = [M] + m_1 \begin{bmatrix} 1 & H_c \\ H_c & H_c^2 \end{bmatrix}, \tag{23d}$$

$$[M] = \begin{bmatrix} m_1 & m_1 H_c \\ m_1 H_c & m_1 H_c^2 + I_1 \end{bmatrix} \tag{23e}$$

for the superstructure:

$$U_1 = \frac{m_1\omega^2}{K_{\mathrm{str}} + \mathrm{i}\omega C_{\mathrm{str}} - m_1\omega^2}(U_0 + H_c\Phi_0). \tag{24}$$

Eqs. (23) and (24) provide the solution in closed form. The computations, however, may be somewhat tedious if performed by hand, since K matrix involves complex numbers. On the other hand, it is noted that if a real-number notation (with amplitudes and phase angles) had been adopted (as in Eq. (15)), Eqs. (23) would become six equations with six unknowns—a less desirable procedure. A simple computer code could readily perform the operations in Eqs. (23) and (24).

3.2. Computing dynamic impedances: tables and charts for dynamic "springs" and "dashpots"

The most important geometric and material factors affecting the dynamic impedance of a foundation are:

(1) the foundation shape (circular, strip, rectangular, arbitrary),
(2) the type of soil profile (deep uniform or multi-layer deposit, shallow stratum on rock),
(3) the embedment (surface foundation, embedded foundation, pile foundation).

For a project of critical significance a case-specific analysis must be performed, using the most suitable numerical computer program. In most practical cases, however, foundation impedances can be estimated from approximate expressions and charts. For the usual case of a practically rigid foundation, a number of analytical formulae and charts for such stiffnesses have been

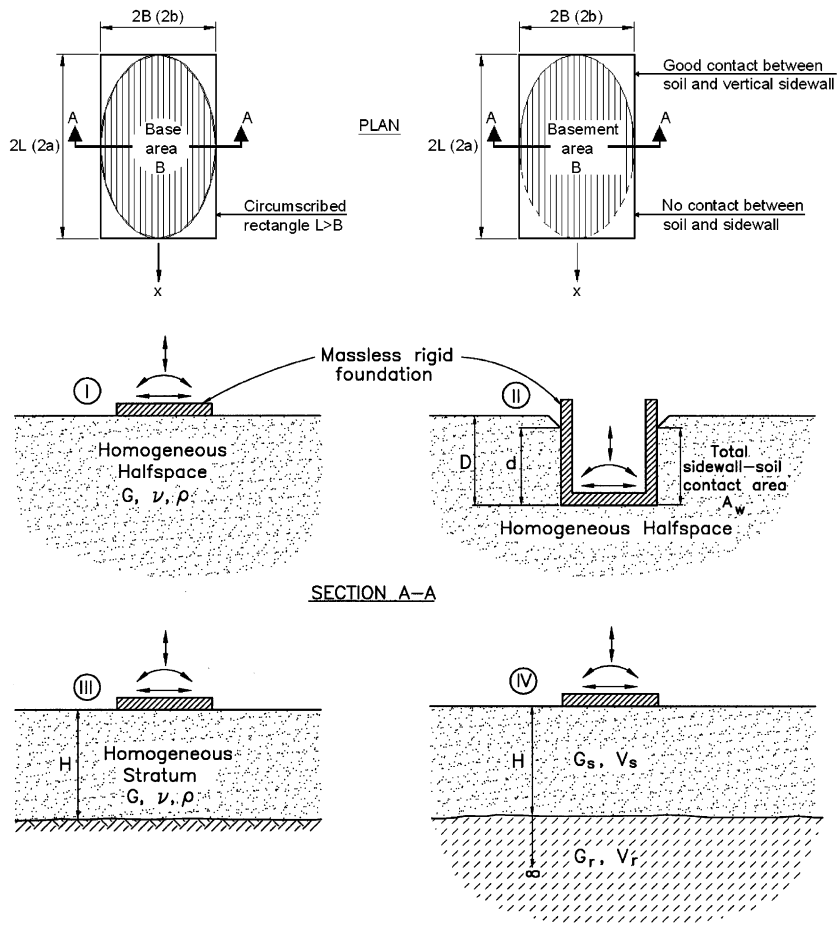

Fig. 7. The four foundation–soil systems whose impedances are given in tabular/graphical form. Numbers I–IV refer to corresponding tables and the associated graphs.

published (e.g., [24,28–35]) and are presented in this section.

3.3. Surface foundation on homogeneous halfspace

For an arbitrarily-shaped foundation mat, the engineer must first determine an "equivalent" circumscribed rectangle $2B$ by $2L$ ($L > B$) using common sense, as sketched in Fig. 7. Then, to compute the impedances in the six modes of vibration from Table 1a, all that is needed is:

- A_b, I_{bx}, I_{by}, I_b are area, moments of inertia about x, y, and polar moment of inertia about z, of the actual soil foundation contact surface; if loss of contact under part of the foundation (e.g. along the edges of a rocking foundation) is likely, engineering judgment may be used to discount the contribution of this part.
- B and L are semi-width and semi length of the circumscribed rectangle.
- G, ν, V_s and V_{La}, the shear modulus, Poisson's ratio, shear wave velocity, and "Lysmer's analog" wave velocity; the latter is the apparent propagation velocity of compression–extension waves under a foundation and is related to V_s according to

$$V_{La} = \frac{3.4}{\pi(1-\nu)} V_s. \tag{25}$$

Additional discussion on the Lysmer analog velocity can be found in Ref. [33].

- ω = cyclic frequency (in rad/s) of interest.

This table as well as all other tables in this paper gives:

- the dynamic stiffness ("springs"), $\bar{K} = \bar{K}(\omega)$ as a product of the static stiffness, K, times the dynamic stiffness coefficient $k = k(\omega)$:

$$\bar{K}(\omega) = K \times k(\omega), \tag{26}$$

- the radiation damping ("dashpot") coefficient $C = C(\omega)$. These coefficients do not include the soil hysteretic damping, β. To incorporate such damping, one should simply add to the foregoing C value the corresponding material dashpot coefficient $2\bar{K}\beta/\omega$:

$$\text{total } C = \text{radiation } C + \frac{2\bar{K}\beta}{\omega}. \tag{27}$$

The special cases of footings of rectangular and elliptic shape are addressed in Table 1b.

Table 1a
Dynamic stiffness and dashpot coefficients for arbitrary shaped foundations on homogenous halfspace surface

Vibration mode	Dynamic stiffness $\mathscr{K} = Kk(\omega)$			Radiation dashpot coefficient C
	Static stiffness K		Dynamic stiffness coefficient k	(General shapes)
	General shape (foundation–soil contact surface area $= A_b$ with equivalent rectangle $2L \times 2B$; $L > B$)[a]	Square $L = B$	(General shape; $0 \leqslant a_0 \leqslant 2$)[b]	
Vertical, z	$K_z = \frac{2GL}{1-\nu}(0.73 + 1.54\chi^{0.75})$ with $\chi = \frac{A_b}{4L^2}$	$K_z = \frac{4.54GB}{1-\nu}$	$k_z = k_z\left(\frac{L}{B}, \nu, a_0\right)$ plotted in Graph a	$C_z = (\rho V_{La} A_b)\bar{c}_z$ $\bar{c}_z = \bar{c}_z\left(\frac{L}{B}, a_0\right)$ plotted in Graph c
Horizontal, y (lateral direction)	$K_y = \frac{2GL}{2-\nu}(2 + 2.5\chi^{0.85})$	$K_y = \frac{9GB}{2-\nu}$	$k_y = k_y\left(\frac{L}{B}, a_0\right)$ plotted in Graph b	$C_y = (\rho V_s A_b)\bar{c}_y$ $\bar{c}_y = \bar{c}_y\left(\frac{L}{B}, a_0\right)$ plotted in Graph d
Horizontal, x (longitudinal direction)	$K_x = K_y - \frac{0.2}{0.75-\nu} GL\left(1 - \frac{B}{L}\right)$	$K_x = K_y$	$k_x \simeq 1$	$C_x \simeq \rho V_s A_b$
Rocking, rx (around x axis)	$K_{rx} = \frac{G}{1-\nu} / \underset{bx}{0.75} \left(\frac{L}{B}\right)^{0.25} \left(2.4 + 0.5\frac{B}{L}\right)$ with I_{bx} = area moment of inertia of foundation–soil contact surface around x axis	$K_{rx} = \frac{0.45GB^3}{1-\nu}$	$k_{rx} = 1 - 0.20a_0$	$C_{rx} = (\rho V_{La} I_{bx})\bar{c}_{rx}$ $\bar{c}_{rx} = \bar{c}_{rx}\left(\frac{L}{B}, a_0\right)$ plotted in Graph e
Rocking, ry (around y axis)	$K_{ry} = \frac{G}{1-\nu} / \underset{by}{0.75} \left[3\left(\frac{L}{B}\right)^{0.15}\right]$ with I_{by} = area moment of inertia of foundation–soil contact surface around y axis	$K_{ry} = K_{rx}$	$\begin{cases} \nu < 0.45; \\ k_{ry} \simeq 1 - 0.30a_0 \\ \nu \simeq 0.5: \\ k_{ry} \simeq 1 - 0.25a_0\left(\frac{L}{B}\right)^{0.30} \end{cases}$	$C_{ry} = (\rho V_{La} I_{by})\bar{c}_{ry}$ $\bar{c}_{ry} = \bar{c}_{ry}\left(\frac{L}{B}, a_0\right)$ plotted in Graph f
Torsional	$K_t = GJ_t^{0.75}\left[4 + 11\left(1 - \frac{B}{L}\right)^{10}\right]$ with $J_t = I_{bx} + I_{by}$ polar moment of inertia of foundation–soil contact surface	$K_t = 8.3GB^3$	$k_t \simeq 1 - 0.14a_0$	$C_t = (\rho V_s J_t)\bar{c}_t$ $\bar{c}_t = \bar{c}_t\left(\frac{L}{B}, a_0\right)$ plotted in Graph g

[a]Note that as $L/B \to \infty$ (strip footing) the theoretical values of K_z and $K_y \to 0$; values computed from the two given formulas correspond to footing of $L/B \approx 20$.
[b]$a_0 = \omega B / V_s$.

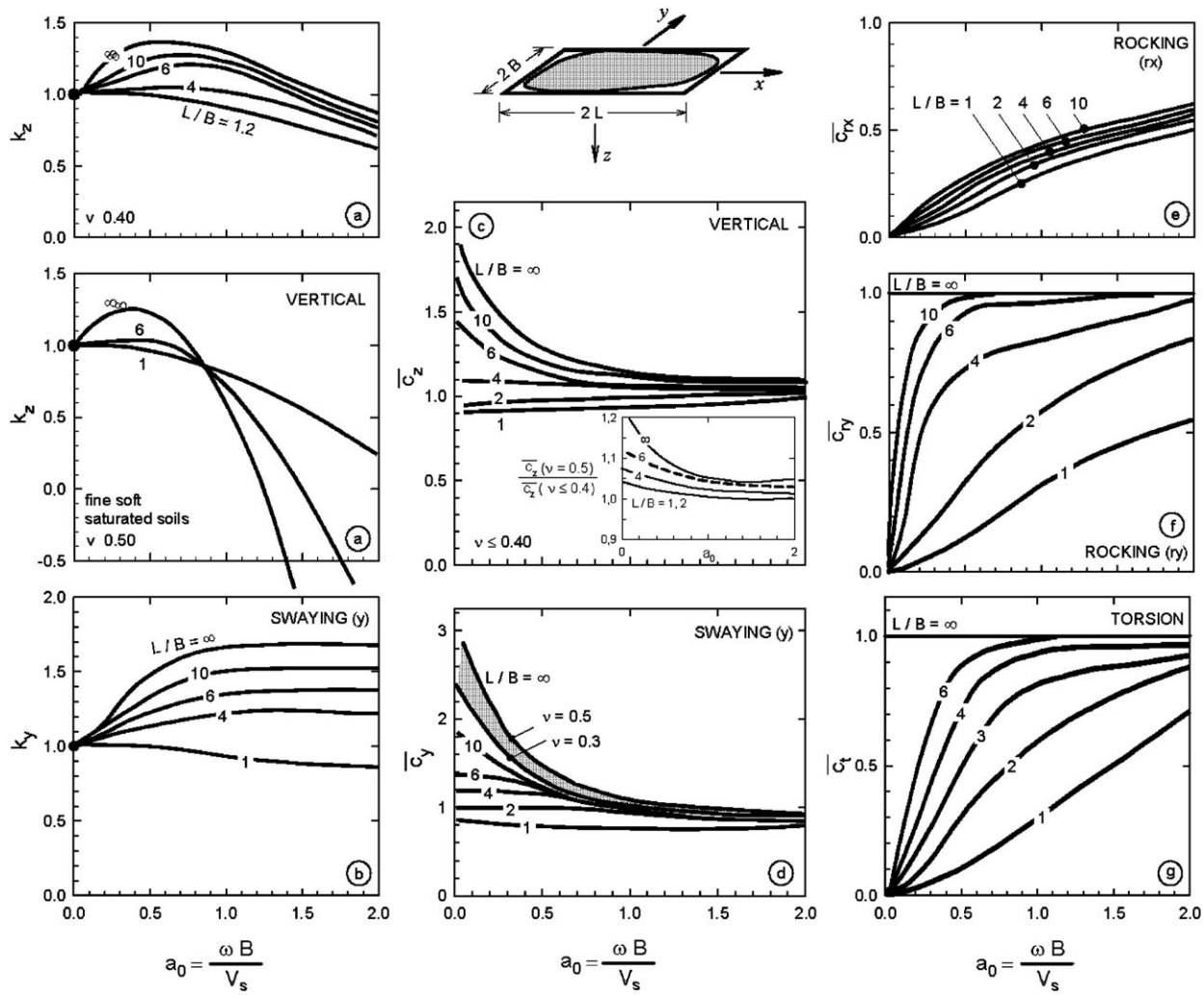

Table 1b
Stiffness for foundations of rectangular and elliptical shape on homogeneous halfspace surface

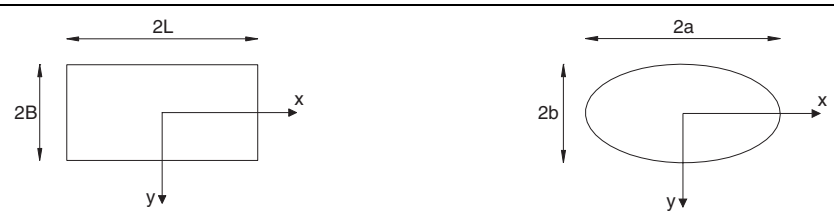

Response mode	Static stiffness K			
	Rectangle ($B/L = 2$)	Rectangle ($B/L = 4$)	Ellipse ($a/b = 2$)	Ellipse ($a/b = 4$)
Vertical, z	$K_z = \frac{3.3GL}{1-\nu}$	$\frac{2.55GL}{1-\nu}$	$\frac{2.9Ga}{1-\nu}$	$\frac{1.8Ga}{1-\nu}$
Horizontal, y (lateral direction)	$K_y = \frac{6.8GL}{2-\nu}$	$\frac{5.54GL}{2-\nu}$	$\frac{6.5Ga}{2-\nu}$	$\frac{5.3Ga}{2-\nu}$
Horizontal, x (longitudinal direction)	$K_x = \frac{4.9(1-1.4\nu)}{(2-\nu)(0.75-\nu)}GL$	$\frac{3.9(1-1.4\nu)}{(2-\nu)(0.75-\nu)}GL$	$\frac{4.7(1-1.37\nu)}{(2-\nu)(0.75-\nu)}Ga$	$\frac{3.7(1-1.4\nu)}{(2-\nu)(0.75-\nu)}Ga$
Rocking, rx (around x axis)	$K_{rx} = \frac{0.82GL^3}{1-\nu}$	$\frac{0.2GL^3}{1-\nu}$	$\frac{0.55Ga^3}{1-\nu}$	$\frac{0.78Ga^3}{1-\nu}$
Rocking, ry (around y axis)	$K_{ry} = \frac{2.46GL^3}{1-\nu}$	$\frac{1.62GL^3}{1-\nu}$	$\frac{1.65Ga^3}{1-\nu}$	$\frac{1.1Ga^3}{1-\nu}$
Torsional	$K_t = 3.5GL^3$	$2.1GL^3$	$2.35Ga^3$	$1.4Ga^3$

3.4. Partially and fully embedded foundations

For a foundation embedded in a deep and relatively homogeneous soil deposit that can be modeled as a homogeneous halfspace, springs and dashpots are obtained from the formulae and charts of Table 2a (modified from Gazetas [36]). The foundation basemat can again be of arbitrary (solid) shape (Fig. 7). The engineer must determine the following additional parameters using the table:

- D is the depth below the ground surface of the foundation basemat.
- A_w or d is the total area of the actual sidewall–soil contact surface, or the (average) height of the sidewall that is in good contact with the surrounding soil. A_w should, in general, be smaller that the nominal area of contact to account for such phenomena as slippage and separation that may occur near the ground surface. The engineer should refer to published results of large and small-scale experiments for a guidance in selecting a suitable value for A_w or d (e.g., [37–40]). Note that A_w or d will not necessarily attain a single value for all modes of vibration.
- A_{ws} and A_{wce} which refer to horizontal oscillations and represent the sum of the projections of all the sidewall area in directions parallel (A_{ws}) and perpendicular (A_{wce}) to loading. Again A_{ws} and A_{wce} should be smaller than the nominal areas in shearing and compression, to account for slippage and/or separation. h is the distance of the (effective) sidewall centroid from the ground surface.
- Note that most of the formulae of Table 2a are valid for symmetric and nonsymmetric contact along the perimeter of the vertical sidewalls and the surrounding soil. Note also that Table 2a compares the dynamic stiffnesses and dashpot coefficients of an embedded foundation $\bar{K}_{emb} = \bar{K}_{emb} \times k_{emb}$ and C_{emb} with those of the corresponding surface foundation, $\bar{K}_{sur} = \bar{K}_{sur} \times k_{sur}$ and C_{sur}.

Approximate solutions for the special cases of footings of rectangular and elliptic shapes are given in Table 2b.

3.5. Presence of bedrock at shallow depth

Natural soil deposits are frequently underlain by very stiff material or bedrock at a shallow depth, rather than extending to practically infinite depth as the homogenous halfspace implies. The proximity of such stiff formation to the oscillating surface modifies the static stiffness, K, and dashpot coefficients $C(\omega)$. Specifically, with reference to Table 3 and its charts:

(a) The static stiffnesses in all modes decrease with the relative depth to bedrock H/B. This is evident from all formulae of Table 3, which reduce to the corresponding halfspace stiffnesses when H/R approaches infinity.

Particularly sensitive to variations in the depth to rock are the vertical stiffnesses—the effect being far more pronounced with strip footings (factor 3.5 versus 1.3). Horizontal stiffnesses are also appreciably affected. On the other hand, for $H/R > 1.5$ the response to torsional loads is essentially independent of the layer thickness.

As indication of the causes of this different behavior (between circular and strip footings and, in any footing, between the different types of loading) can be obtained by comparing the depths of the "zone of influence" in each case. Circular and square foundations on a homogeneous halfspace induce vertical normal stresses σ_z along the centerline of the footing that become practically negligible at depths exceeding 5 footing radii ($z_v = 5R$); with strip foundations vertical stresses practically vanish only below 15 footing widths ($z_v = 15B$). The depth of influence, z_h, for the horizontal stresses τ_{zx}, due to lateral loading is about $2R$ and $6B$ for circle and strip, respectively. On the other hand, for all foundation shapes (strip, rectangle, circle), moment loading is "felt" down to a depth, z_r, of about $2B$ or $2R$. For torsion, finally $z_t = 0.75R$ or $0.75B$.

Apparently when a rigid formation extends into the "zone of influence" of a particular loading mode, it eliminates the corresponding deformations and thereby increases the stiffness.

(b) The variation of the dynamic stiffness coefficients with frequency reveals an equally strong dependence on the depth to bedrock H/B. On a stratum, $k(\omega)$ is not a smooth function but exhibits undulations (peaks and valleys) associated with the natural frequencies (in shearing and compression–extension) of the stratum. In other words, the observed fluctuations are the outcome of resonance phenomena: waves emanating from the oscillating foundation reflect at the soil–bedrock interface and return back to their source at the surface. As a result, the amplitude of the foundation motion may significantly increase at frequencies near the natural frequencies of the deposit. Thus, the dynamic stiffness (being the inverse of displacements) exhibits troughs, which can be very steep when the hysteretic damping of the soil is small (in fact, in certain cases, $k(\omega)$ would be exactly zero if the soil was ideally elastic).

For the "shearing" modes of vibration (swaying and torsion) the natural fundamental frequency of the stratum which controls the behavior of $k(\omega)$ is

$$f_s = \frac{V_s}{4H}, \tag{28}$$

where H denotes the thickness of the layer, while for the "compressing" modes (vertical, rocking) the corresponding frequency is

$$f_c = \frac{V_{L\alpha}}{4H} = \frac{3.4}{\pi(1-\nu)} f_s. \tag{29}$$

(c) The variation of the dashpot coefficient, C, with frequency reveals a twofold effect on the presence of a rigid base at relatively shallow depth. First, $C(\omega)$ also exhibits undulations (crests and troughs) due to the wave reflections

Table 2a
Dynamic stiffnesses and dashpot coefficients for arbitrary shaped foundations partially or fully embedded in a homogeneous halfspace

Vibration mode	Dynamic stiffness $\mathscr{K}_{\text{emb}} = K_{\text{emb}} k_{\text{emb}}(\omega)$		Radiation dashpot coefficient $C_{\text{emb}}(\omega)$	
	Static stiffness K_{emb} (foundation with arbitrarily-shaped basemat A_{b} with equivalent rectangle $2L \times 2B$; total sidewall–soil contact area A_{w} (or constant wall–solid contact height d)	Dynamic stiffness coefficient $k_{\text{emb}}(\omega)$ $(0 \leqslant a_0 \leqslant 2)$	General foundation shape	Rectangular foundation $2L \times 2B \times d$
Vertical z	$K_{z,\text{emb}} = K_{z,\text{surf}}\left[1 + \frac{1}{21}\frac{D}{B}(1 + 1.3\chi)\right] \times \left[1 + 0.2\left(\frac{A_{\text{w}}}{A_{\text{b}}}\right)^{2/3}\right]$	$\nu \leqslant 0.4$ Fully embedded : $K_{z,\text{emb}} = K_{z,\text{surf}}\left[1 - 0.09\left(\frac{D}{B}\right)^{3/4} a_0^2\right]$ In a trench $K_{z,\text{tre}} = K_{z,\text{surf}}\left[1 + 0.09\left(\frac{D}{B}\right)^{3/4} a_0^2\right]$ Partially embedded : interpolate between the two	$C_{z,\text{emb}} = C_{z,\text{surf}} + \rho V_{\text{s}} A_w$	$C_{z,\text{emb}} = 4\rho V_{\text{La}} BL\bar{c}_z + 4\rho V_{\text{s}}(B + L)d$
	$K_{z,\text{surf}}$ obtained from Table 1 A_{w} = actual sidewall–soild contact area; for constant effective contact high d along the perimeter $A_{\text{w}} = d \times$ Perimeter $\chi = A_{\text{b}}/4L^2$	$\nu = 0.5$ Fully embedded, $L/B \simeq 1 - 2$ $K_{z,\text{emb}} \simeq 1 - 0.09\left(\frac{D}{B}\right)^{3/4} a_0^2$ Fully embedded, $L/B > 3$ $K_{z,\text{emb}} \simeq 1 - 0.35\left(\frac{D}{B}\right)^{1/2} a_0^{0.35}$	$C_{z,\text{surf}}$: see Table 1	$\bar{c}_z$ according to Table 1
Horizontal y or x	$K_{y,\text{emb}} = K_{y,\text{surf}}\left(1 + 0.15\sqrt{\frac{D}{B}}\right) \times \left[1 + 0.52\left(\frac{h}{B}\frac{A_{\text{w}}}{L^2}\right)^{0.4}\right]$	$K_{y,\text{emb}}$ and $K_{x,\text{emb}}$ can be estimated in term of L/D, D/B, and d/B for each a_0 from the grant accompanying this table	$C_{y,\text{emb}} = C_{y,\text{surf}} + \rho V_{\text{s}} A_{\text{ws}} + \rho V_{\text{La}} A_{\text{wce}}$	$C_{y,\text{emb}} = 4\rho V_{\text{s}} BL\bar{c}_y + 4\rho V_{\text{s}} Bd + 4\rho V_{\text{Ls}} Ld$
	$K_{y,\text{surf}}$ obtained from Table 1 $K_{x,\text{emb}}$ and $C_{x,\text{emb}}$ are computed similarly from $K_{x,\text{surf}}$ and $C_{y,\text{surf}}$		$A_{\text{ws}} = \sum(A_{\text{wi}} \sin \vartheta_i)$ = total effective sidewall area shearing the soil $A_{\text{wce}} = \sum(A_{\text{wi}} \cos \vartheta_i)$ = total effective sideall area compressing the soil θ = inclination angle of surface A_{wi} from loading direction $C_{y,\text{surf}}$ according to Table 1	$\bar{c}_y$ according to Table 1

Table 2a (*continued*)

Vibration mode	Dynamic stiffness $\mathscr{K}_{\text{emb}} = K_{\text{emb}} k_{\text{emb}}(\omega)$		Radiation dashpot coefficient $C_{\text{emb}}(\omega)$	
	Static stiffness K_{emb} (foundation with arbitrarily-shaped basemat A_{b} with equivalent rectangle $2L \times 2B$; total sidewall–soil contact area A_{w} (or constant wall–solid contact height d)	Dynamic stiffness coefficient $k_{\text{emb}}(\omega)$ $(0 \leqslant a_0 \leqslant 2)$	General foundation shape	Rectangular foundation $2L \times 2B \times d$
Rocking rx (around long axis)	Expressions valid for any basemat shape but constant effective contact height d along the perimeter $K_{\text{r}x,\text{emb}} = K_{\text{r}x,\text{surf}} \times \left\{1 + 1.26\frac{d}{B}\left[1 + \frac{d}{B}\left(\frac{d}{D}\right)^{-0.2}\sqrt{\frac{B}{L}}\right]\right\}$	$K_{\text{r}x,\text{emb}} \simeq K_{\text{r}x,\text{surf}}$ $K_{\text{r}y,\text{emb}} \simeq K_{\text{r}y,\text{surf}}$	$C_{\text{r}x,\text{emb}} = C_{\text{r}x,\text{sur}} + \rho V_{\text{La}} I_{\text{wce}} \bar{c}_1 + \rho V_{\text{s}}(J_{\text{ws}} + \sum[A_{\text{wcei}} \Delta_i^2])\bar{c}_1$ $\bar{c}_1 = 0.25 + 0.65\sqrt{a_0}\left(\frac{d}{B}\right)^{-a_0/2}\left(\frac{d}{B}\right)^{-1/4}$ I_{wce} = total moment of inertia about their base axis parallel to x of all sidewall surfaces effectively compressing the soil Δ_i = distance of surface A_{wcei} from x axis J_{ws} = polar moment of inertia about their base axis parallel to x of all sidewall surfaces effectively shearing the soil	$C_{\text{r}x,\text{emb}} = \frac{4}{3}\rho V_{\text{La}} B^3 L \bar{c}_{\text{r}x} + \frac{4}{3}\rho V_{\text{La}} d^3 L \bar{c}_1 + \frac{4}{3}\rho V_{\text{s}} B d(B^2 + d^2)\bar{c}_1 + 4\rho V_{\text{s}} B^2 d L \bar{c}_1$
Rocking ry (around lateral axis)	$K_{\text{r}y,\text{emb}} = K_{\text{r}y,\text{surf}} \times \left\{1 + 0.92\left(\frac{d}{B}\right)^{0.6}\left[1.5 + \left(\frac{d}{D}\right)^{1.9}\left(\frac{B}{L}\right)^{-0.6}\right]\right\}$		$C_{\text{r}y,\text{emb}}$ is similarly evaluated from $C_{\text{r}y,\text{sur}}$ with y replacing x and, in the equation for c_1, L replacing B	with $\bar{c}_1$ as in the preceding column and $\bar{c}_{\text{r}x}$ according to Table 1
Coupling term Swaying-rocking x, ry Swaying-rocking y, rx	$K_{x\text{r}y,\text{emb}} \simeq \frac{1}{3} d K_{x,\text{emb}}$ $K_{y\text{r}x,\text{emb}} \simeq \frac{1}{3} d K_{y,\text{emb}}$	$K_{x\text{r}y,\text{emb}} \simeq K_{y\text{r}x,\text{emb}} \simeq 1$	$C_{x\text{r}y,\text{emb}} \simeq \frac{1}{3} d C_{x,\text{emb}}$ $C_{y\text{r}x,\text{emb}} \simeq \frac{1}{3} d C_{y,\text{emb}}$	As in the previous column
Torsional	$K_{\text{t},\text{emb}} = K_{\text{t},\text{surf}} \times \left[1 + 1.4\left(1 + \frac{B}{L}\right)\left(\frac{d}{B}\right)^{0.9}\right]$	$K_{\text{t},\text{emb}} \simeq K_{\text{t},\text{surf}}$	$C_{\text{t},\text{emb}} = C_{\text{t},\text{sur}} + \rho V_{\text{La}} J_{\text{wce}} \bar{c}_2 + \rho V_{\text{s}} \sum[A_{\text{wi}} \Delta_i^2]\bar{c}_2$ $\bar{c}_2 \approx \left(\frac{d}{D}\right)^{-0.5} a_0^2\left[a_0^2 + \frac{1}{2}(L/B)^{-1.5}\right]^{-1}$ J_{wce} = total moment of inertia of all sidewall surfaces compressing the soil about the projection of z axis onto their plane Δ_{zi} = distance of surface A_{wi} from z axis	$C_{\text{t},\text{emb}} = \frac{4}{3}\rho V_{\text{s}} BL(B^2 + L^2)\bar{c}_{\text{t}} + \frac{4}{3}\rho V_{\text{La}} d(L^3 + B^3)\bar{c}_2 + 4\rho V_{\text{s}} dBL(B + L)\bar{c}_2$ with $\bar{c}_2$ as in the preceding column and $\bar{c}_{\text{t}}$ according to Table 1

[a]Note that as $L/B \to \infty$ (strip footing) the theoretical values of K_z $K_y \to 0$; values computed from the two given formulas correspond to footing of $L/B \approx 20$.
[b]$a_0 = \omega B / V_{\text{s}}$.

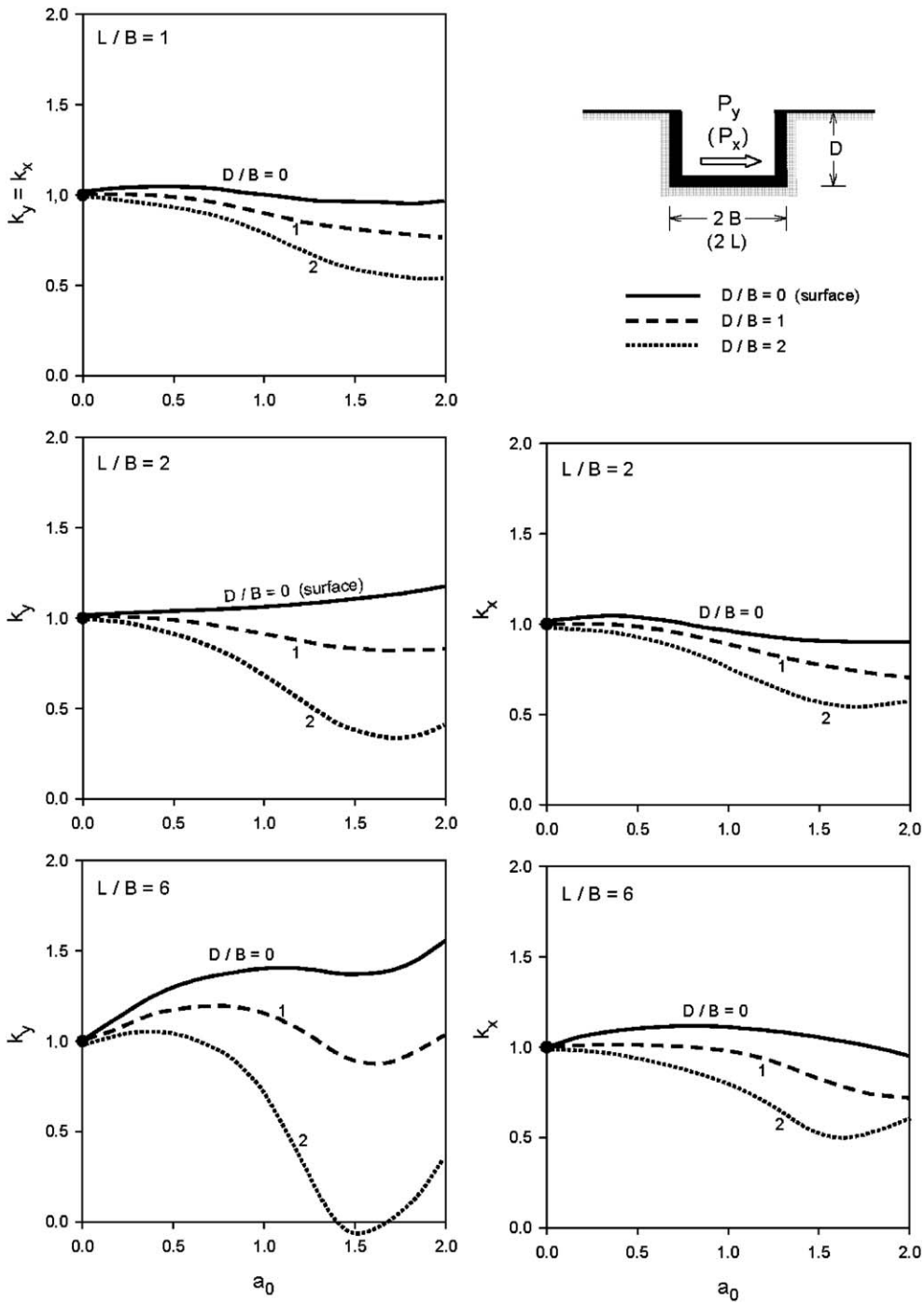

at the rigid boundary. These fluctuations are more pronounced with strip than with circular foundations, but are not as significant as for the corresponding stiffness $k(\omega)$. Second, and far more important from a practical viewpoint, is that at low frequencies below the first resonant ("cutoff") frequency of each mode of vibration, radiation damping is zero or negligible for all shapes of footings and all modes of vibration. This is due to the fact that no surface waves can exist in a soil stratum over bedrock at such low frequencies; and, since the bedrock also prevents waves from propagating downward, the overall radiation of wave energy from the footing is negligible or nonexistent.

Such an elimination of radiation damping may have severe consequences for heavy foundations oscillating vertically or horizontally, which would have experienced substantial amounts of damping in a very deep deposit (halfspace)—recall illustrative examples for Tables 1a and 2a. On the other hand, since the low-frequency values of C in rocking and torsion are small even in a halfspace, operating below the cutoff frequencies may not change appreciably from the presence of bedrock.

Table 2b
Stiffness for foundations of rectangular and elliptical shape embedded in homogeneous halfspace

Response mode	Static stiffness K			
	Rectangle ($B/L=2$)	Rectangle ($B/L=4$)	Ellipse ($a/b=2$)	Ellipse ($a/b=4$)
Vertical, z	$K_{z,\mathrm{emb}}=K_{z,\mathrm{surf}}\times\chi_z$			
	$\chi_z=\left(1+0.16\frac{D}{L}\right)\times\left[1+0.42\left(\frac{d}{L}\right)^{2/3}\right]$	$\left(1+0.25\frac{D}{L}\right)\times\left[1+0.6\left(\frac{d}{L}\right)^{2/3}\right]$	$\left(1+0.14\frac{D}{a}\right)\times\left[1+0.42\left(\frac{d}{a}\right)^{2/3}\right]$	$\left(1+0.24\frac{D}{a}\right)\times\left[1+0.6\left(\frac{d}{a}\right)^{2/3}\right]$
Horizontal, y (lateral direction)	$K_{y,\mathrm{emb}}=K_{y,\mathrm{surf}}\times\chi_y$			
	$\chi_y=\left(1+0.2\sqrt{\frac{D}{L}}\right)\times\left[1+\left(\frac{d}{L}\right)^{0.8}\right]$	$\left(1+0.3\sqrt{\frac{D}{L}}\right)\times\left[1+1.3\left(\frac{d}{L}\right)^{0.8}\right]$	$\left(1+0.2\sqrt{\frac{D}{a}}\right)\times\left[1+\left(\frac{d}{a}\right)^{0.8}\right]$	$\left(1+0.3\sqrt{\frac{D}{a}}\right)\times\left[1+1.2\left(\frac{d}{a}\right)^{0.8}\right]$
Rocking, rx (around x axis)	$K_{\mathrm{r}x,\mathrm{emb}}=K_{\mathrm{r}x,\mathrm{surf}}\times\chi_{\mathrm{r}x}$			
	$\chi_{\mathrm{r}x}=1+2.5\frac{d}{L}\left[1+1.4\frac{d}{L}\left(\frac{d}{D}\right)^{-0.2}\right]$	$1+5\frac{d}{L}\times\left[1+2\frac{d}{L}\left(\frac{d}{D}\right)^{-0.2}\right]$	$1+2.5\frac{d}{a}\times\left[1+1.4\frac{d}{a}\left(\frac{d}{D}\right)^{-0.2}\right]$	$1+5\frac{d}{a}\times\left[1+2\frac{d}{a}\left(\frac{d}{D}\right)^{-0.2}\right]$
Rocking, ry (around y axis)	$K_{\mathrm{r}y,\mathrm{emb}}=K_{\mathrm{r}y,\mathrm{surf}}\times\chi_{\mathrm{r}y}$			
	$\chi_{\mathrm{r}y}=1+2.1\left(\frac{d}{L}\right)^{0.6}\left[1+\left(\frac{d}{D}\right)^{1.9}\right]$	$1+3.2\left(\frac{d}{L}\right)^{0.6}\times\left[1+1.5\left(\frac{d}{D}\right)^{1.9}\right]$	$1+2\left(\frac{d}{a}\right)^{0.6}\times\left[1+\left(\frac{d}{D}\right)^{1.9}\right]$	$1+3.2\left(\frac{d}{a}\right)^{0.6}\times\left[1+1.5\left(\frac{d}{D}\right)^{1.9}\right]$
Torsional	$K_{\mathrm{t,emb}}=K_{\mathrm{t,surf}}\times\chi_{\mathrm{t}}$			
	$\chi_{\mathrm{t}}=1+3.7\left(\frac{d}{L}\right)^{0.9}$	$1+6.1\left(\frac{d}{L}\right)^{0.9}$	$1+4\left(\frac{d}{a}\right)^{0.9}$	$1+6\left(\frac{d}{a}\right)^{0.9}$

Note: $K_{*,\mathrm{surf}}$ obtained from Table 1b.

Note that at operating frequencies f beyond f_s or f_c, as appropriate for each mode, the "stratum" damping fluctuates about the halfspace damping C ($H/B=\infty$). The "amplitude" of such fluctuations tends to decrease with increasing H/B. Moreover, if some wave energy penetrates into bedrock (as it does happen in real life thanks to some weathering of the upper masses of rock) the fluctuations tend to wither away—hence the recommendation of Table 3.

3.6. Foundations on soil stratum over halfspace

The homogeneous halfspace and the stratum-on-rigid-base are two idealizations of extreme soil profiles. A more realistic soil model, the stratum over halfspace, is studied in this subsection. Besides the H/R or H/B ratio, the ratio G_s/G_r (or the wave velocity ration V_s/V_r) is needed to describe such a soil model. When G_s/G_r tends to zero the stratum-on-rigid base ("bedrock") is recovered; when it becomes equal to 1, the model reduces to a homogeneous halfspace. For intermediate situations of $0<G_s/G_r<1$, springs and dashpots can be estimated using the information of this paragraph.

Table 4 presents formulas for the static stiffness of circular and strip foundations, in terms of G_s/G_r and H/R (for the circle) or H/B (for the strip). These formulas are valid for $G_s\leqslant G_r$, i.e., a halfspace stiffer than the layer. At the lower limit, $G_s/G_r\to 0$, the expressions reduce to those of Table 3 for a layer on rigid base. At the upper limit, $G_s/G_r\to 1$, the halfspace expressions (Table 1) are recovered. At intermediate values, as the rigidity of the supporting halfspace decreases, the static stiffnesses of the foundation decrease, apparently due to increasing magnitude of strains in the halfspace. The results are intuitively obvious and need no further explanation.

The dynamic stiffness and damping coefficients as functions of frequency also exhibit intermediate behavior between those for halfspace and for stratum over bedrock. Thus the observed undulations are not as sharp as the undulations on a stratum over bedrock, depending, of course, on the value of G_s/G_r.

In general, compared to a stratum over bedrock, the flexibility of the base layer (halfspace) produces a *decrease* in stiffness but an *increase* in radiation damping. The latter stems from the fact that waves emitted from the foundation–soil interface penetrate into the halfspace, rather than being fully reflected.

For the earthquake problem, this increase in radiation damping is practically most significant for the swaying dashpot at frequencies $\omega=2\pi f$ below the fundamental frequency of the *top* soil stratum. Recall that at such frequencies, when the halfspace is a rigid bedrock, no radiation damping can generate, and hence resonance amplifications in the seismic response may develop. In this case this is no longer true. Fig. 8 gives a chart for estimating the swaying dashpot C_y for several values of the ratio V_s/V_r. This chart applies to circular or square foundations with $H/R\approx 3$–4 and for strip foundations with $H/B=2$. The chart can only be used as a guide in other cases.

On the other hand, rotational modes of vibration generate little damping below their respective cutoff frequencies, and the significance of rock flexibility is of minor practical significance. This is also true for higher frequencies, since "destructive" interference of waves emitted from a rotating (in rocking or torsion) foundation limits the depth these waves can reach. Hence the flexibility or rigidity of the base layer is, again, of practically little significance.

Additional information on this topic can be found in [24,28,41,42].

Table 3
Dynamic stiffness and dashpot coefficients for surface foundations on homogeneous stratum over bedrock

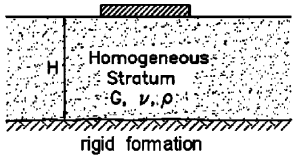

Foundation shape		Circular foundation of radius $B = R$	Rectangular foundation $2B$ by $2L$ ($L > B$)	Strip foundation $2L \to \infty$
Static stiffness	Vertical, z	$K_z = \frac{4GR}{1-\nu}\left(1 + 1.3\frac{R}{H}\right)$	$K_z = \frac{2GL}{1-\nu}\left[0.73 + 1.54\left(\frac{B}{L}\right)^{3/4}\right]\left(1 + \frac{B/H}{0.5+B/L}\right)$	$\frac{K_z}{2L} \approx \frac{0.73G}{1-\nu}\left(1 + 3.5\frac{B}{H}\right)$
K	Horizontal, y	$K_y = \frac{8GR}{2-\nu}\left(1 + 0.5\frac{R}{H}\right)$	*	$\frac{K_y}{2L} \approx \frac{2G}{2-\nu}\left(1 + 2\frac{B}{H}\right)$
	Horizontal, x	$K_x = K_y$	*	–
	Rocking, rx	$K_{rx} = \frac{8GR^3}{3(1-\nu)}\left(1 + 0.17\frac{R}{H}\right)$	*	$\frac{K_{rx}}{2L} = \frac{\pi GB^2}{2(1-\nu)}\left(1 + 0.2\frac{B}{H}\right)$
	Rocking, ry	$K_{rx} = K_{ry}$	*	–
	Torsional, t	$K_t = \frac{16GR^3}{3}\left(1 + 0.10\frac{R}{H}\right)$	*	–
Dynamic stiffness coefficient $k(\omega)$	Vertical, z	$k_z = k_z(H/R, a_0)$ is obtained from Graph III-1	$k_z = k_z(H/B, L/B, a_0)$ is plotted in Graph III-2 for rectangles and strip	
	Horizontal, y or x	$k_y = k_y(H/R, a_0)$ is obtained from Graph III-1	*	$k_y = k_y(H/B, a_0)$ is obtained from Graph III-3
	Rocking, rx or ry	$k_\alpha(H/R) \approx k_\alpha(\infty)$	*	$k_{rx} \approx k_{rx}(\infty)$
	Torsional, t	$\alpha = rx, ry, t$	*	
Radiation dashpot coefficient $C(\omega)$	Vertical, z	$C_z(H/B) \approx 0$ at $f < f_c$; regardless of foundation shape $C_z(H/B) \approx 0.8\ C_z(\infty)$ at $f \geqslant 1.5\ f_c$ At intermediate frequencies: interpolate linearly. $f_c = \frac{V_{La}}{4H}$, $V_{La} = \frac{3.4V_s}{\pi(1-\nu)}$		
	Horizontal, y or x	$C_y(H/B) \approx 0$ at $f < \frac{3}{4}f_s$; $C_y(H/B) \approx C_y(\infty)$ at $f > \frac{4}{3}f_s$ Similarly for C_x At intermediate frequencies: interpolate linearly. $f_s = \frac{V_s}{4H}$		
	Rocking, rx or ry	$C_{rx}(H/B) \approx 0$ at $f < f_c$; $C_{rx}(H/B) \approx C_{rx}(\infty)$ at $f > f_c$ Similarly for C_{ry}		
	Torsional, t	$C_t(H/B) \approx C_t(\infty)$		

*Not available.

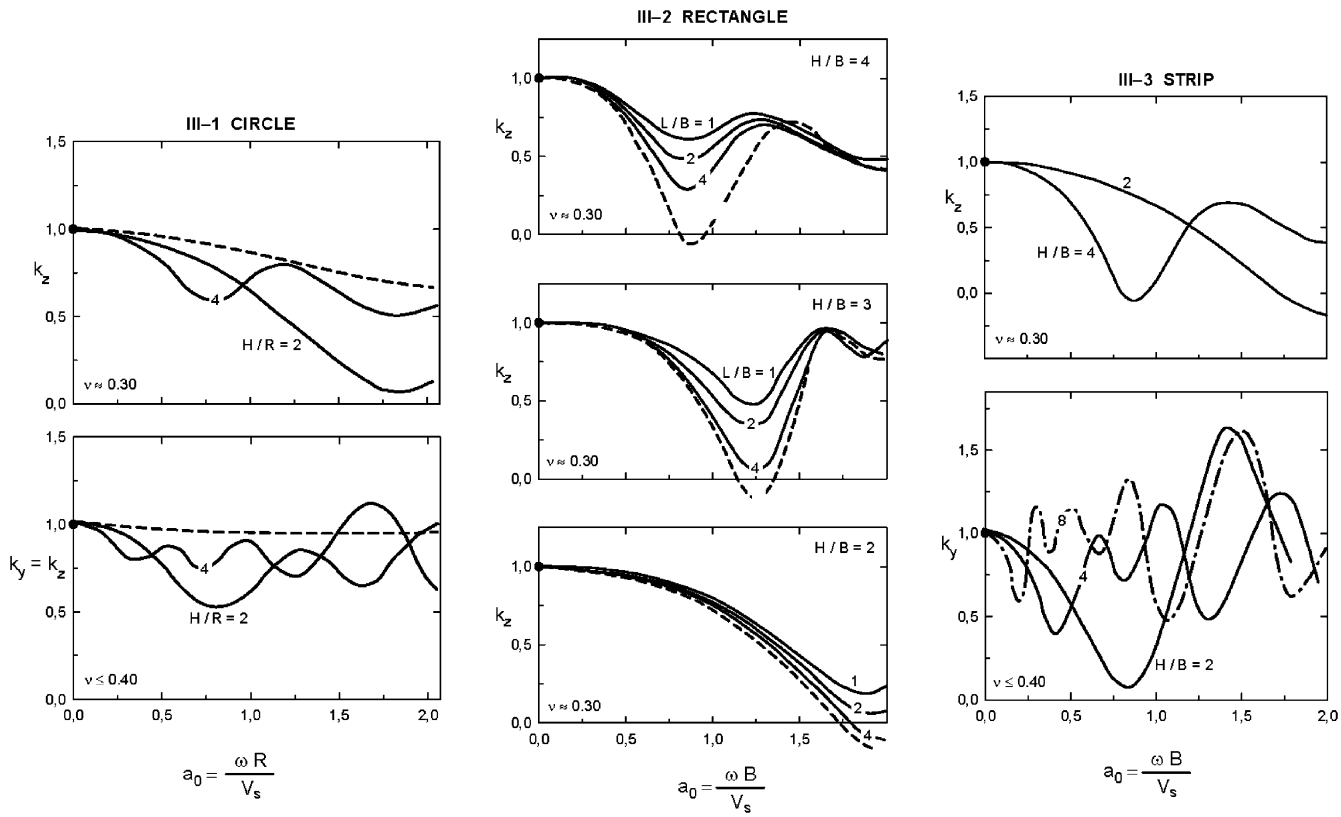

Table 4
Static stiffness of circular and strip foundations on soil stratum over halfspace

Vibration mode	General expression $K = K(G_s/G_r, H/B) = K(1,\infty) \times \frac{1+m(B/H)}{1+m(B/H)(G_s/G_r)}$		
	$K(1,\infty)$	m	
		Circle	Strip
Vertical	K	1.3	3.5
Horizontal	of homogenous halfspace	0.5	2.0
Torsional		0.17	0.2

3.7. Effect of soil heterogeneity

The assumption of homogeneous or layered halfspace may not be realistic in practice, as the soil gets progressively stiffer with depth, even in uniform deposits. The prime cause is the increase in confining pressure with depth and the associated increase in low-strain shear modulus. Soil inhomogeneity can be easily treated in dynamic finite-element formulations by dividing the soil into a number of homogeneous layers. Yet, such formulations have not been adequately exploited to study parametrically the dynamic behavior of foundations [43]. On the other hand, there is an inherent difficulty in applying analytical and semi-analytical methods to dynamics of inhomogeneous media, because of the difficulties associated with decoupling of the governing equations and solving of the related differential equations with variable coefficients. As a result, the number of solutions available today is limited [32,33,44–47].

In this paper information is provided on three specific cases for which solutions are available:

- A rectangular footing with side lengths $2L$ and $2B$ ($L > B$) resting on an elastic deposit with shear modulus increasing with depth as

$$G = G_0 + (G_\infty - G_0)(1 - e^{-b(z/B)}), \tag{30}$$

where G_0 and G_∞ denote the shear moduli at the surface and at infinite depth, respectively, and b is a dimensionless inhomogeneity constant. The problem has been analysed by Vrettos [33] for the case of vertical and rocking oscillations.
- A circular footing of radius R oscillating vertically on elastic soil with shear modulus increasing proportionally to the square of depth, and Poisson's ratio v equal to 0.25 [32]

$$G = G_0\left(1 + b\frac{z}{R}\right)^2. \tag{31}$$

b is a dimensionless inhomogeneity parameter which can be determined by fitting pertinent experimental results or field data. The corresponding problem of a strip footing has been solved by Gazetas [46] and is not discussed here. This model can simulate deposits with a fast increase in elastic modulus. Usually, however, the quadratic G-variation in Eq. (31) is of minor importance for practical applications.

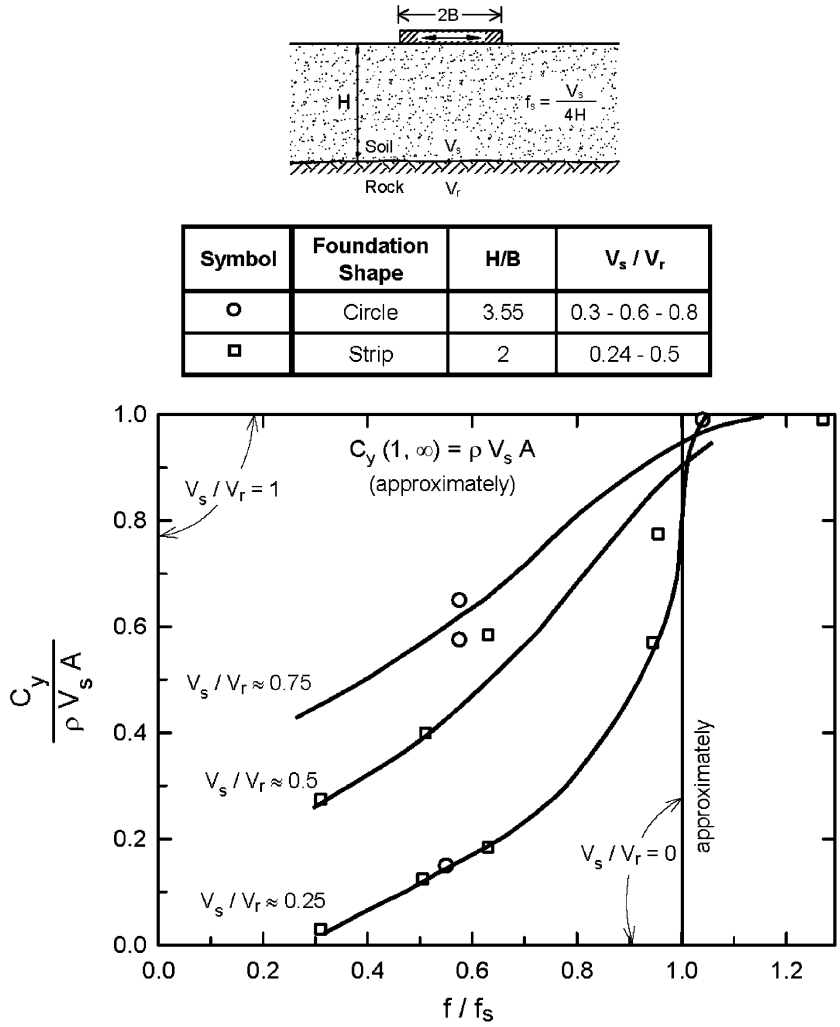

Fig. 8. Horizontal radiation dashpot C_y of a foundation on a soil layer underlain by "flexible" rock, as a fraction of the homogeneous halfspace value C_y $(1,\infty)$, for various ratios V_S/V_r (after Dobry and Gazetas [39]).

Table 5
Static stiffness for rigid rectangular foundations (after Vrettos [33])

Ξ_0	v	b	L/B	$K_z/G_0\ B$	$K_{ry}/G_0\ B^3$	$K_{rx}/G_0\ B^3$
0	0.3		1	6.373	5.370	5.370
			2	9.326	9.610	27.044
			4	14.277	13.992	144.047
0	0.2		1	5.576	4.699	4.699
	0.45			8.111	6.835	6.835
0.5	0.3	0.5	1	9.188	6.508	6.508
			2	14.113	11.842	35.174
			4	22.556	22.422	201.029
0.5	0.3	1	1	10.115	7.180	7.180
		1.5		10.636	7.653	7.653
0.5	0.2	0.5	1	7.908	5.630	5.630
		1		8.694	6.183	6.183
0.5	0.45	0.5	1	12.154	8.507	8.507
		1		13.420	9.486	9.486
0.7	0.3	0.25	1	10.469	6.824	6.824
		0.5		12.314	7.812	7.812
		1		14.458	9.246	9.246
0.9	0.3	0.1	1	13.092	7.600	7.600

- A circular footing or radius R oscillating vertically on elastic soil with shear modulus increasing according to the function [24]

$$G = G_0\left(1 + b\frac{z}{R}\right)^n, \tag{32}$$

where n and b are dimensionless parameters.

With reference to the profile in Eq. (30), Table 5 presents results for static stiffnesses in the vertical and rocking modes for different values of the soil Poisson's ratio. In the table, Ξ_0 denotes the dimensionless parameter

$$\Xi_0 = 1 - \frac{G_0}{G_\infty}, \tag{33}$$

which is bounded by zero and one. Selected results for dynamic stiffness and dashpots coefficients are presented in Fig. 9. The dimensionless frequency factor indicated in the graph is expressed in terms of the shear wave velocity at the surface (V_{so}) (Table 6).

For the footing on the profile described by Eq. (31), dynamic stiffness and dashpot coefficients are depicted in Fig. 10. Corresponding static stiffnesses are provided in the paper by Guzina and Pak [32] and in [48]. It is noted that material damping in the soil has been ignored in all the above studies and, thereby, the derived dashpot coefficients pertain only to wave radiation.

The following noteworthy trends can be identified in these figures:

1. The variation with frequency of dynamic stiffness is smaller in a heterogeneous soil than in a homogeneous soil. In addition, the dynamic stiffness coefficient k generally decreases with increasing levels of inhomogeneity. The differences, however, are of secondary importance from a practical point of view.

2. Radiation damping decreases substantially with increasing inhomogeneity in the soil. The effect is more pronounced at low frequencies. This decrease is understood given the limited ability of an inhomogeneous medium to radiate waves away from the source [24,45]. At high frequencies the discrepancies in damping between an inhomogeneous and a homogeneous medium become smaller. This can be explained considering that high frequency (small wavelength) waves emitted from the foundation "see" the medium as a homogeneous halfspace having wave velocity equal to the *surface* velocity V_{so} (in shearing) or V_{Lao} (in compression–extension). This property has been utilized in the development of "cone" models for related problems [14,49].

Table 6
Values of G/G_{max} for soil beneath foundations (from NEHRP-2003 and EC8)

	Spectral response acceleration, SA			
	$\leqslant 0.10$	$\leqslant 0.15$	0.20	$\geqslant 0.30$
G/G_{max}	0.81	0.64	0.49	0.42

The fact that soil stiffness does not appear as variable in this table [e.g., at least through a soil category] reduces dramatically its usefulness.

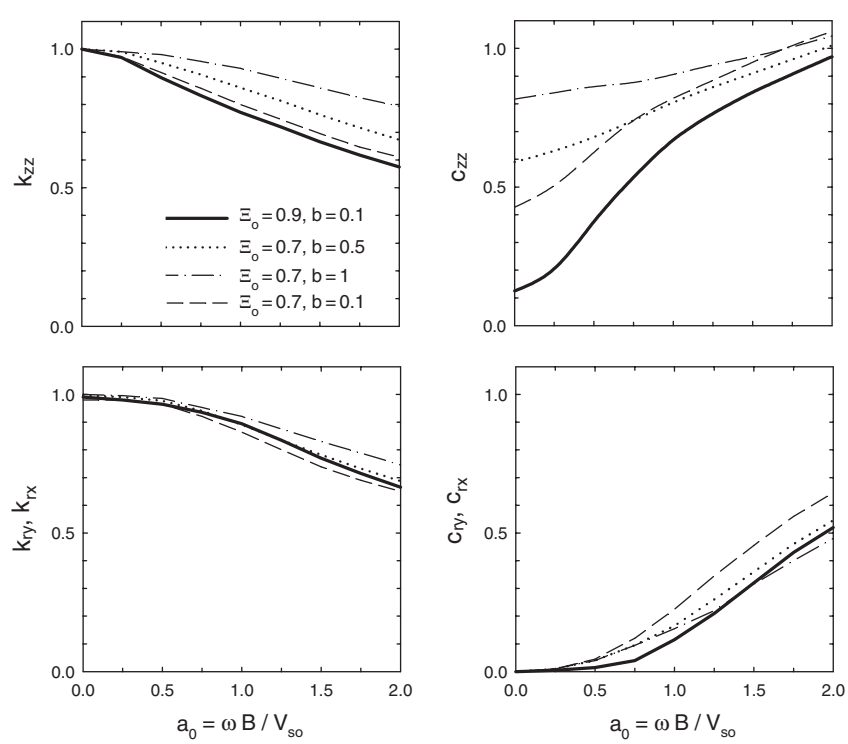

Fig. 9. Normalized dynamic stiffness and dashpot coefficients for vertical and rocking motion of a square foundation on a nonhomogeneous soil for different values of b and Ξ_0 (modified from [33]).

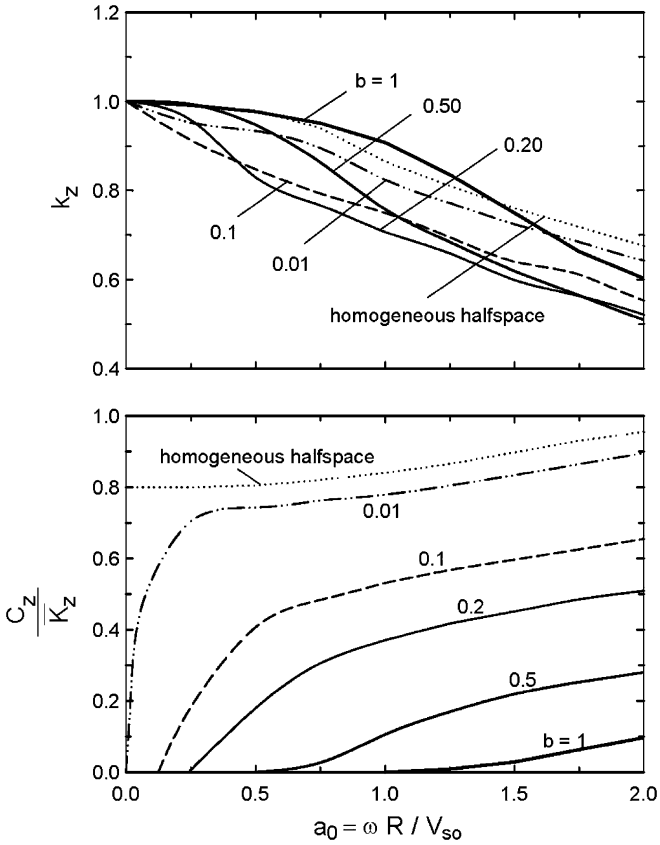

Fig. 10. Dynamic spring and dashpot coefficient for a rigid circular footing on a linear wave-velocity halfspace (modified from [32]).

3. A cutoff frequency is apparent in the results for the circular footing in Fig. 10. As pointed out by Guzina and Pak [32], this may not be totally surprising, since the profile can be regarded as a limiting case of a multi-layered medium in which wave reflections can occur at the "interfaces" in the vertical direction. An interesting discussion on the issue of cutoff frequency is given in [50].

To develop further insight on the effect of inhomogeneity in radiation damping, Fig. 11 depicts radiation damping expressed in terms of the ratio

$$\beta_{ij}(\omega) = \frac{\omega C_{ij}(\omega)}{2\bar{K}_{ij}(\omega)}. \tag{34}$$

The above ratio is referred to as "damping performance index" and is analogous to the critical damping ratio in the theory of the single-degree-of-freedom oscillator. In Fig. 11, the dramatic decrease in radiation damping resulting from soil inhomogeneity becomes clearly evident.

3.8. Effect of soil nonlinearity

In current soil–structure interaction (SSI) practice, nonlinear plastic soil behavior is usually approximated through a series of iterative linear analyses, using soil properties (moduli and damping ratios) that are consistent with the level of shearing strains resulting from the previous analysis [5,52]. These analyses may utilize a wealth of available experimental soil data relating the decrease in (secant) shear modulus and the increase in

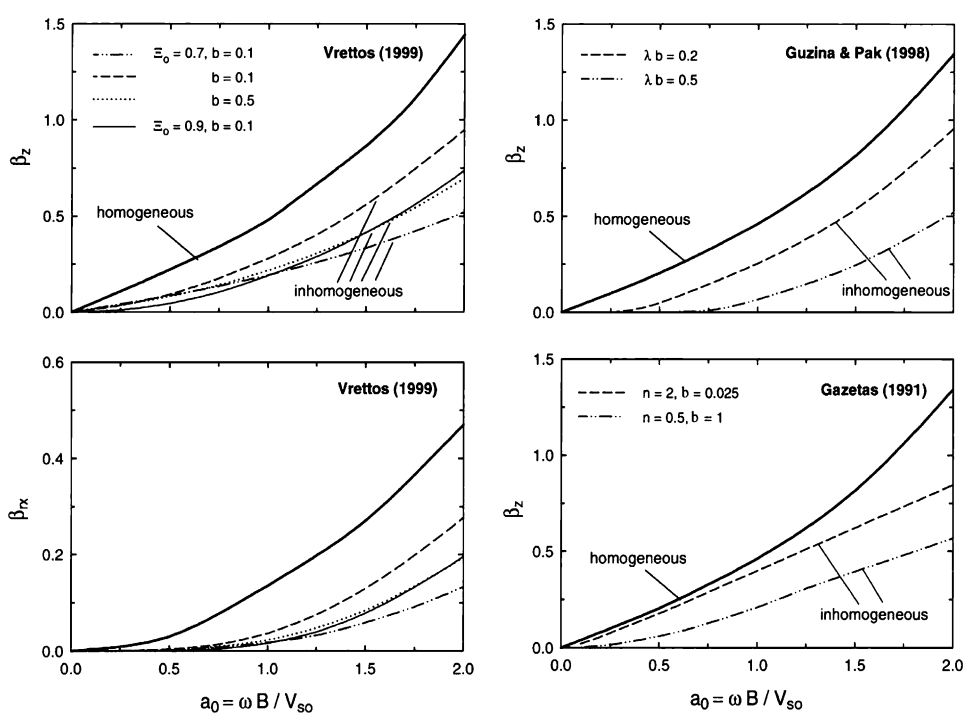

Fig. 11. Effect of inhomogeneity on normalized damping for vertical (upper left) and rocking motion (lower left) of a square footing based on Vrettos [33]; vertical motion of circular footing based on Guzina and Pak [32] and Gazetas [51].

(effective) damping ratio with increasing amplitude of shear strain.

Nonlinearities in the free-field soil are treated routinely with programs such as SHAKE [6,53]. Much less work has been reported on nonlinearities on the dynamic impedance functions of footings. In one of the few available studies (e.g., [54–56]), Borja [54] reports that soil nonlinearity resulting from an external harmonic load tends to increase the foundation motion and generate low-frequency resonances even in a homogeneous halfspace. Another interesting study has been conducted by Jakub and Roesset [57]. In this, the soil is modeled as homogeneous or inhomogeneous stratum over rigid base with $H/B = 1$, 2, and 4. A Ramber-Osgood model was used to simulate the nonlinear constitutive relations of soil and iterative linear analyses were performed. One of the two parameters of the Ramber-Osgood model, r, was kept constant equal to 2, while the second one, α, was varied so as to cover a wide range of typical soil stress–strain relations. In this model, the variation of secant modulus and effective damping ratio with stress amplitude is given by

$$\frac{G}{G_0} = \frac{1}{1 + \alpha(\tau/G_0\gamma_y)}, \tag{35a}$$

$$\beta = \frac{2}{3\pi}\frac{G}{G_0}\frac{\tau}{G_0\gamma_y}, \tag{35b}$$

in which G_0 is the initial shear modulus for low levels of strain; γ_y a characteristic shear strain, typically ranging from 0.0001% to 0.01%; and τ the amplitude of the induced shear stress.

It was concluded that a reasonable approximation to the swaying and rocking impedances of a rigid strip may be obtained from the available linear viscoelastic solutions, provided that the "effective" values of G and β are estimated from Eqs. (35) with

$$\tau = \tau_c, \tag{36}$$

where τ_c is the statically induced shear stress at a depth equal to 0.50 B, immediately below the foundation edge. Note that the above depth coincides with the depth of maximum shear strain under a vertically loaded strip footing [58].

For design purposes and as a first approximation, we mention here that the average shear modulus for the soil beneath a footing can be determined according the NEHRP-2003 recommendations, as a function of the design seismic coefficient of the structure (Table 4). Alternatively, one may use approximate cone models to derive strain-compatible moduli [14].

4. Parametric study of the seismic response of bridge pier

To answer some of the questions raised earlier, a systematic parametric study was conducted on an idealized bridge model. One of features of the study relates to the unavoidable soil nonlinearities during strong seismic excitation. Such nonlinearities are of two types: "*primary*", arising from the shear-wave induced deformations in the free-field soil; and "*secondary*" arising from the stresses induced by the oscillating foundation. Whereas established methods of analysis are available for handling the former type of nonlinearities (through equivalent linear or truly nonlinear algorithms), no simple realistic solution is known for the latter. The approach described above is adopted here and different soil moduli are used for the analysis of wave-propagation and for the computation of the dynamic stiffnesses, consistent with the overall level of strains at characteristic points under the footing. A discussion of the aforementioned decoupling of nonlinearity is given in Ref. [5].

The bridge pier sketched in Fig. 12 is a slightly idealized version of an actual bridge. It involves a single column bent of height $H_c = 6$ m and diameter $d_c = 1.3$ m, founded with a 5-m-diameter ($R = 2.5$ m) footing placed at a depth $D = 3$ m below the ground surface. The axial load carried by the system, $P = 3500$ kN, is typical of a two-lane highway bridge with a span of about 35 m. Considering a shear wave

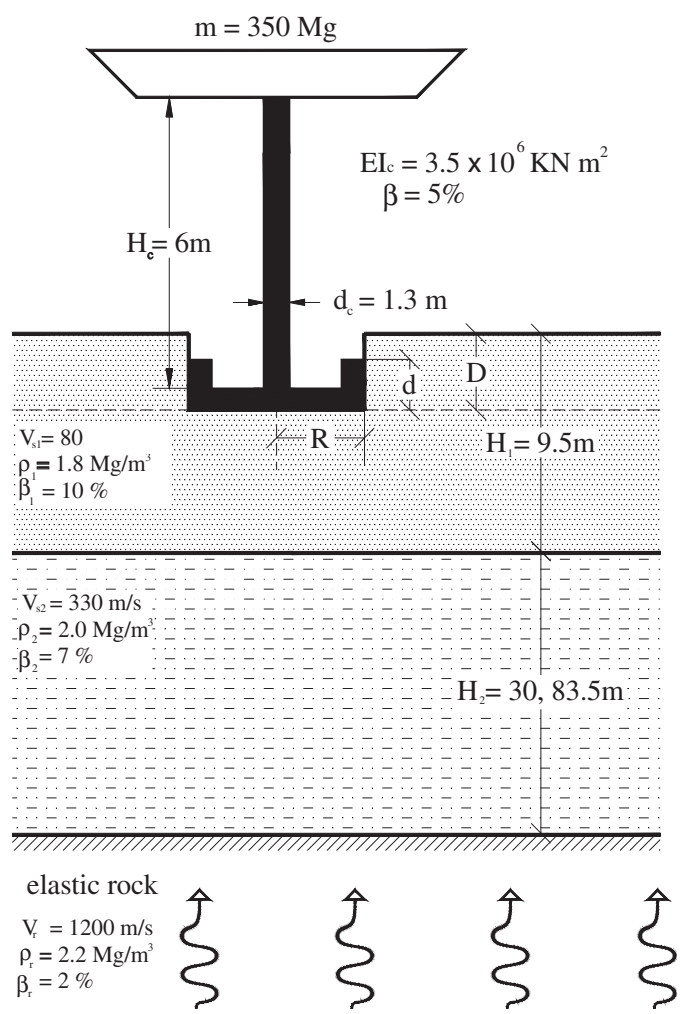

Fig. 12. Bridge system studied.

velocity and a mass density for the top layer of 80 m/s and 2 Mg/m^3, respectively, and using the approximate relation $G/S_u \approx 500$, the undrained shear strength of the top layer is estimated at about 50 kPa. Accordingly, the static factor of safety of the footing is about:

$$\mathrm{FS} \equiv \frac{q_u}{q} = \frac{1.3 \times 5.14 \times 50 + 3 \times 20}{3500/(\pi \times 2.5^2)} \approx 2, \tag{37}$$

which is a sufficient, although marginal, value for a bridge footing.

The contact area between sidewalls and surrounding soil was considered to be either zero (no sidewall–soil contact) or partial sidewall-soil contact over a height $d = 0.5D$ from the base.

Results were obtained for excitation by vertical S waves, described through a horizontal "rock"outcrop motion. Both harmonic steady-state and time-history analyses were performed, in the frequency and time domains, respectively. The former were applied to investigate the salient features (SSI period, effective damping) of the dynamic behavior of the system; the latter were performed to obtain predictions of the response to actual motions. In the time-domain analyses, two different excitation time histories were used, both having a peak horizontal acceleration (PGA) of about 0.40g:

(a) an artificial accelerogram approximately fitted to the NEHRP-94 PGA = 0.4g,
(b) the Pacoima downstream motion, recorded (on "soft rock" outcrop) during the Northridge 1994 earthquake (since the PGA is 0.42g, scaling of this motion was not considered necessary).

The two motions and their five and ten percent damped spectra are shown in Figs. 13 and 14. Use of these motions, as "rock" outcrop excitations, is deemed necessary for checking the limitations (or showing the generality) of our conclusions. The same set of motions has been used by the authors in an earlier study of pile-supported bridge piers [27,59].

The results presented in this section refer to a bridge with a top (deck) free to rotate, subjected to the Pacoima 1994

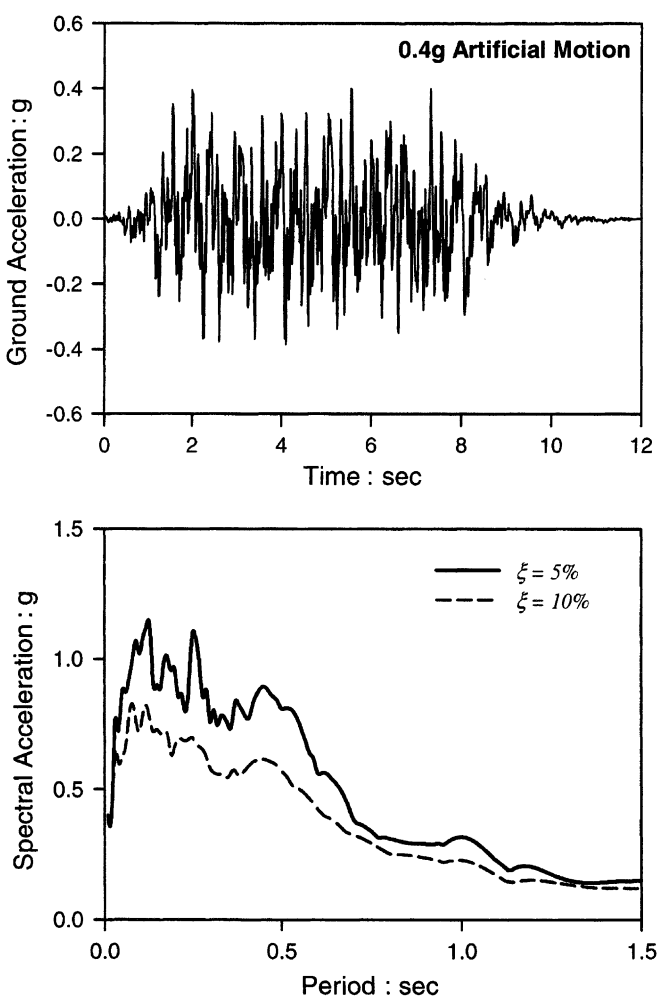

Fig. 13. Artificial 0.4g motion and corresponding response spectra for 5% and 10% damping.

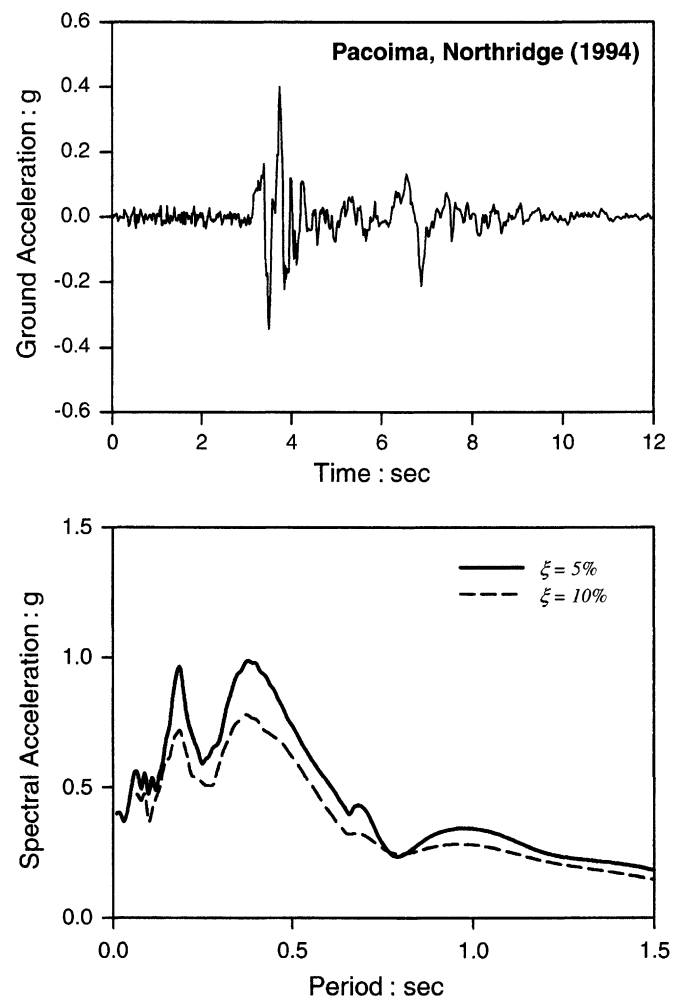

Fig. 14. Pacoima (1994) motion and corresponding response spectra for 5% and 10% damping.

motion, and rigid rock conditions. A second set of parametric results, which incorporate more general boundary conditions, are presented later on.

The harmonic steady state and transient seismic response of this pier, obtained in a complete analysis, is displayed in Figs. 15 and 16. These results should be compared with those in Figs. 17–20, which examine the following cases:

(a) no SSI, i.e. the footing is considered as rigidly supported (Fig. 18)
(b) embedment having partial sidewall contact ($d = 1.5$ m) with the surrounding soil (Figs. 17 and 19)
(c) no radiation damping, i.e. setting for all modes of vibration $C_{\mathrm{rad}} = 0$ (Fig. 20)

The following conclusions can be drawn:

1. Ignoring SSI reduces the fundamental natural period of the system (from 0.83 to 0.53 s), bringing it closer to resonance with the second-mode natural period of the soil deposit (0.48 s). In addition, the effect of the soil radiation and hysteretic damping on the bridge response disappear. Naturally, therefore, the resulting no-SSI bridge transfer functions exhibit a (spurious) sharp and high peak at $T = 0.53$ s.

Moreover, the rock outcrop excitations are richer in the period region of 0.50 s than of 0.80 s, which accentuates the peak at $T = 0.53$ s.

As a result, the no-SSI time histories of bridge-deck and footing accelerations are (Fig. 18), both, nearly *two times larger* than those of the complete solution (with SSI). Also of interest is to notice the change in the nature of the bridge-deck response time histories: the (largest) peak in the complete solution, at $t \approx 4$ s, is in unison with the long-period ground (free field) oscillations occurring after about 3 s—apparently produced by resonance at the fundamental period of the soil deposit. The *early part* of the free-field ground motion, with much shorter periods, is a product of "secondary" resonance between the strong short-period early part of the Pacoima–Northridge excitation and the second natural mode of the soil deposit. However, the effect of this part of the ground motion on the bridge is obviously completely insignificant.

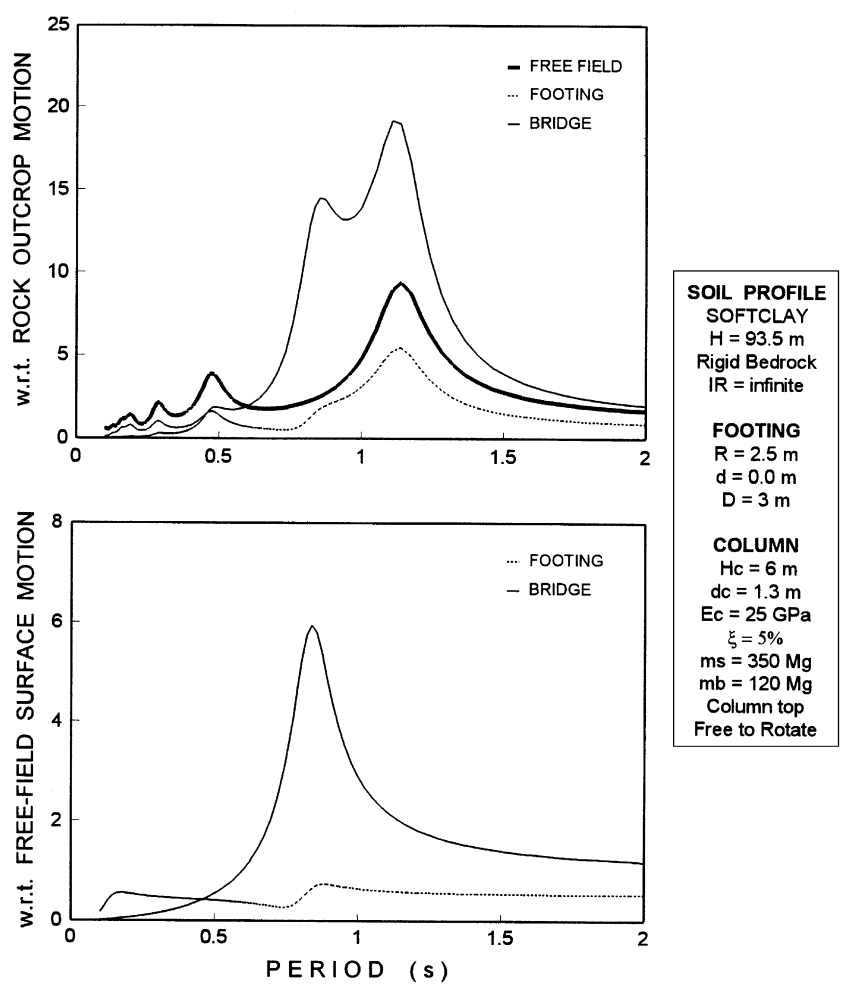

Fig. 15. Complete solution: harmonic steady-state transfer functions.

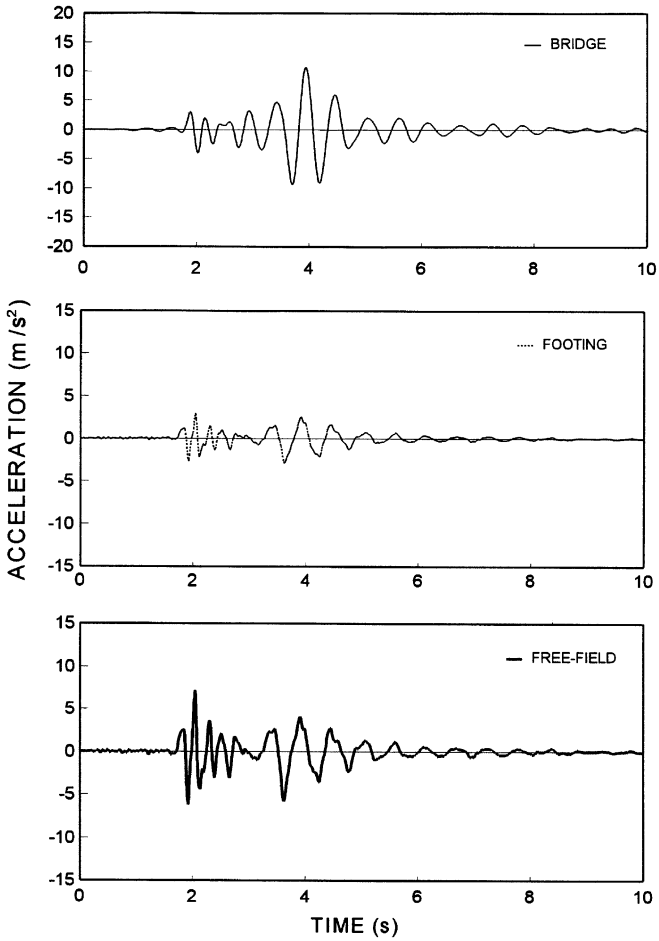

Fig. 16. Complete solution: acceleration histories for Pacoima, Northridge (1994) rock motion.

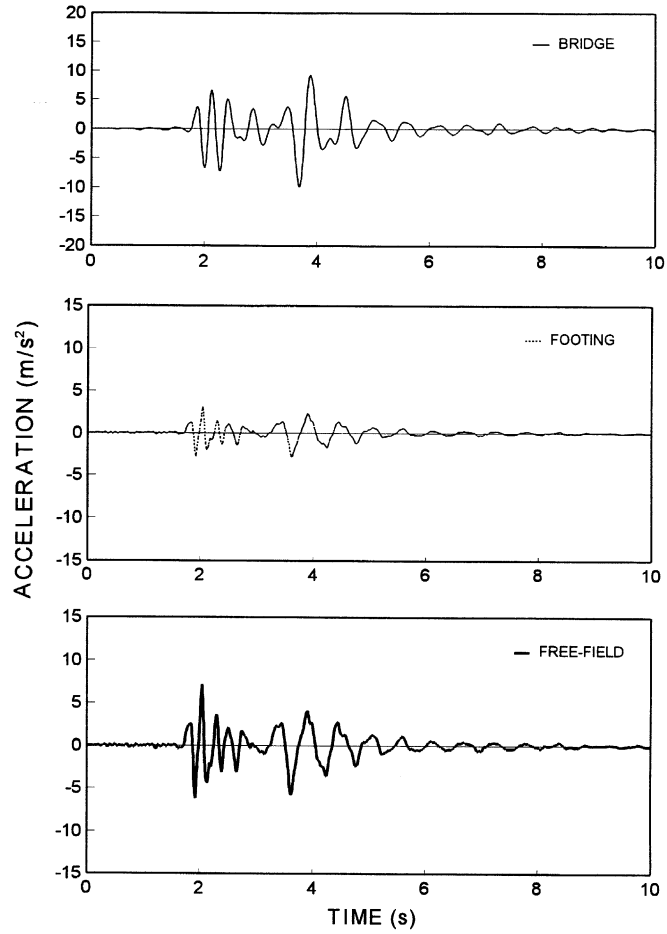

Fig. 17. Solution for improved embedment: acceleration histories for Pacoima, Northridge (1994) rock motion.

The no-SSI response shows exactly the opposite trends, with its (largest) peak occurring at $t \approx 2.5$ s, in phase with the strong ground motion observed at that time.

It should be pointed out that the foregoing trends should not be generalized to *any* bridge-footing system. For example, had the frequency of the earthquake excitation been different (or, alternatively the thickness of the soil profile been smaller or larger), the above trends could be reversed.

3. Neglecting radiation damping in this case has a minor effect both in the frequency and time domains. Two are the reasons: (a) While the fundamental period of the pier considering SSI ($T \approx 0.83$ s) is below the fundamental period of the whole deposit ($T \approx 1.15$ s), the main cutoff period (above which there is little or no radiation damping) is the second natural period corresponding to the resonance of the first (crucial) soft soil layer. Thus, radiation damping in the complete solution is small and neglecting it is of little significance at resonance. (b) In addition, the excitation is not particularly rich in 0.80-s-period components, so even the small decrease in overall damping is of no further consequence. Additional discussion can be found in Refs. [7,60–62].

5. Conclusions

The main conclusions of this study are:

1. The decomposition of SSI into a kinematic (KI) and an inertial (II) part provides a convenient way to analyze the problem. To account for the unavoidable nonlinearities in the soil during strong seismic excitation, it is reasonable (though not strictly correct) to separate soil nonlinearity into "primary", arising from the shear-wave induced deformations in the free-field soil, and "secondary", arising from the stresses induced by the oscillating foundation (which is concentrated close to the surface). Although both phenomena occur simultaneously, in the realm of equivalent linear analyses performed using kinematic and inertial response analyses, different soil moduli can be used in the two steps.

2. KI leads to a foundation input motion (FIM) which is usually smaller than the motion of the free-field soil and, in addition, to a rotational component. Ignoring the rotational excitation may lead to errors on the unsafe side. These errors are small when determining the response of short squatty structures but may be large for tall slender structures. On the other hand, neglecting KI altogether

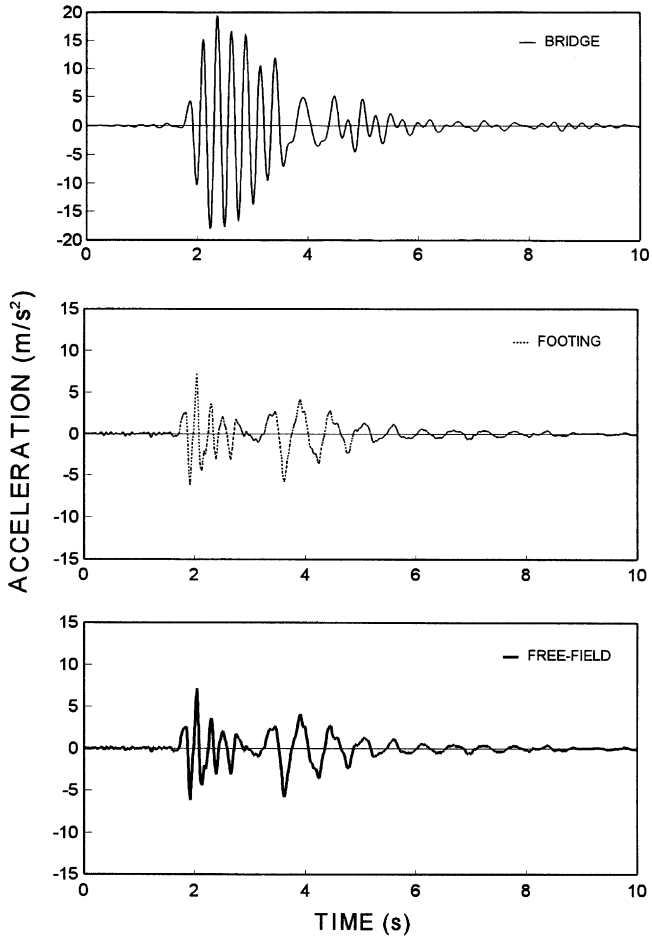

Fig. 18. Solution ignoring SSI: acceleration histories for Pacoima, Northridge (1994) rock motion.

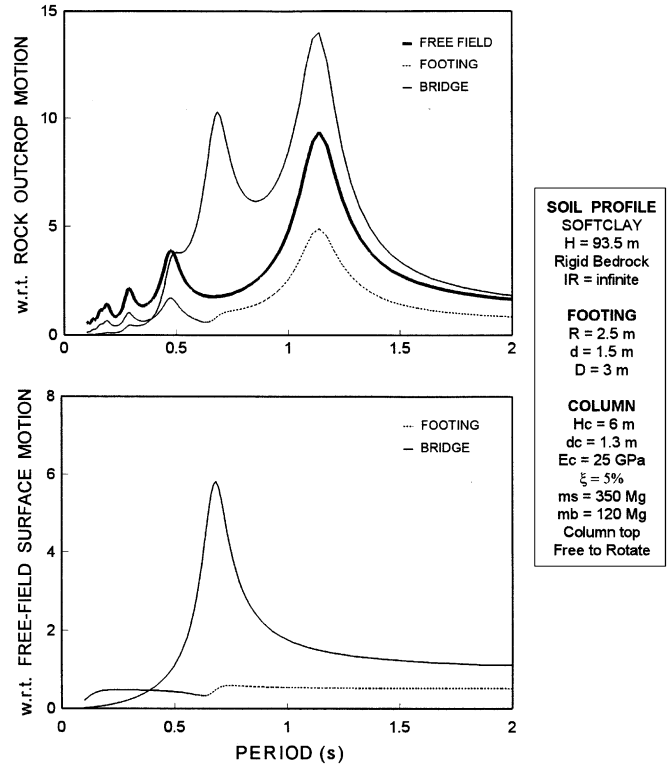

Fig. 19. Solution for improved embedment: harmonic steady-state transfer function.

usually leads to slight conservative results. It is therefore recommended for design of noncritical bridges.

3. In embedded foundations and piles, horizontal forces induce rotational, in addition to translational, oscillations, hence a "cross-coupling" horizontal-rocking impedance exists. Ignoring the coupling stiffness may lead to underestimation of the fundamental period of a flexibly-supported pier. On the other hand, coupling impedances are usually small in shallow foundations and can be ignored.

4. The contact between the sidewalls of an embedded footing and the surrounding soil tends to increase both the stiffness (spring constant) and damping (dashpot constant) of the footing. The actual sidewall area that is in "good" contact with the surrounding soil is usually smaller than the nominal contact area. The actual contact area does not necessarily attain a single value for all modes of vibration.

5. If bedrock is present at a shallow depth beneath a footing, the static stiffness in all modes of vibration increases. Particularly sensitive to the presence of bedrock is the vertical mode. Horizontal stiffnesses may also be appreciably affected. The torsional and rocking stiffnesses remain essentially unaffected.

6. The variation of dynamic stiffness coefficients is also sensitive to the presence of bedrock. The amplitude of the foundation motion may increase significantly at frequencies near the natural frequency of the deposit. Radiation damping is insignificant at frequencies below the "cutoff" frequency of the layer. As with their static counterparts, torsional and rocking damping impedances are not particularly sensitive to the presence of bedrock.

7. The dynamic impedances of footings on a soil stratum overlying a stiffer halfspace exhibit intermediate behavior between those for homogeneous halfspace and for a stratum over bedrock. The flexibility of the halfspace leads to a *decrease* in stiffness but an *increase* in radiation damping. The latter stems from the fact that waves emitted from the foundation–soil interface penetrate into the halfspace rather than being fully reflected. For the earthquake problem, the increase in radiation damping is most significant in the swaying dashpot, at frequencies below the "cutoff" frequency of the stratum.

8. It appears difficult to determine á priori whether SSI will increase or decrease the response of a bridge. In the realm of equivalent linear analyses this seems to be controlled by the following main parameters: (a) The *system damping*: if the fundamental period of the flexibly-supported bridge is significantly smaller than the "cutoff" frequency of the soil (e.g., a rigid pier on a deep and soft deposit), radiation damping will be significant and the response of the system will decrease. In particular, if the cutoff period of the soil is very large (e.g., a thick deposit),

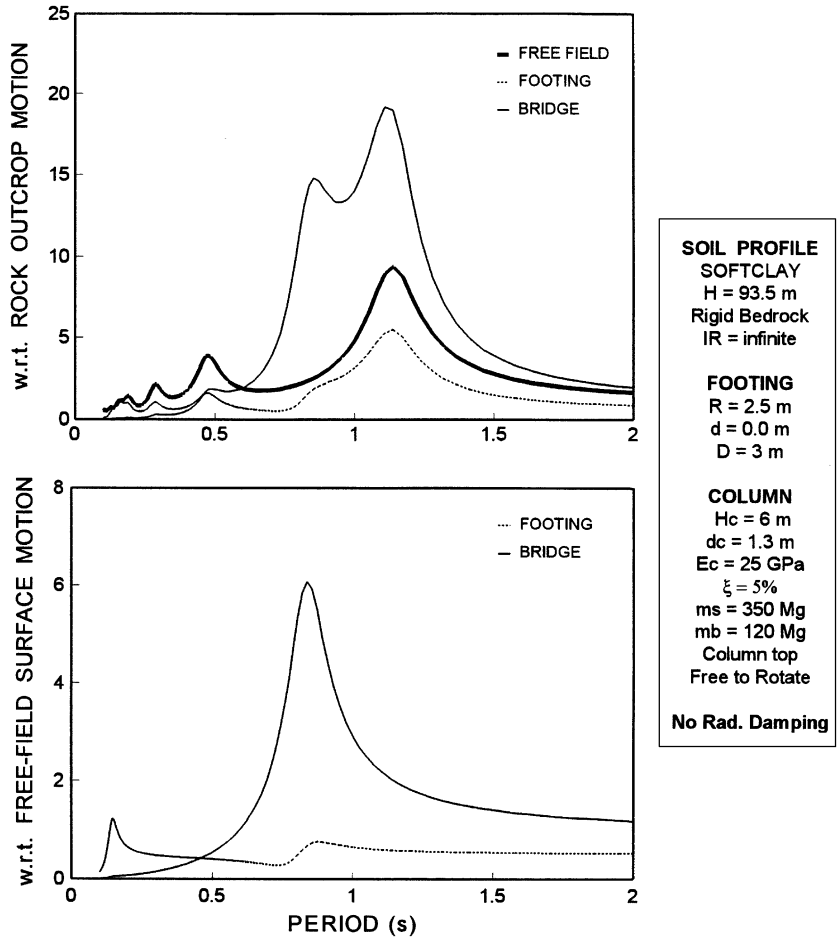

Fig. 20. Solution neglecting radiation damping: harmonic steady-state transfer functions.

radiation damping may be substantial regardless of natural period of the system. This implies that modeling the soil as a halfspace, as done in existing seismic regulations (ATC-3, NEHRP-2003), may lead to *unconservative* estimates of the response. (b) *Resonance between structure and soil.* If the increase in fundamental natural period due to SSI brings the period of the bridge close to an "effective" natural period (especially the first or second) of the soil, resonance will develop which will tend to increase the response. However, if the frequency content of the excitation is not rich in that particular period, the increase may be insignificant. (c) *Double resonance*. If the fundamental natural period of the system coincides with *both* the natural period of the soil and the predominant period of the earthquake motion (at rock level), double resonance will develop (i.e., between structure, soil, and excitation). In this case the response may increase dramatically. Whether or not this will result to damage is related to several additional parameters that are not discussed in this study. (d) *Nonlinear effects*. The development of plastic deformations in the structure and soil, including development of pore water pressure and uplift, may increase the effective natural period of the structure and the soil. This shift in period may lead to either de-resonance or resonance (e.g., bringing the structure closer to the predominant period of the excitation), which, in turn, may lead to "progressive collapse". To date, such strong nonlinearities are beyond the state of the art of seismic SSI.

The conclusions drawn from the parameter studies should not be generalized to bridge piers, soil deposits and seismic excitations with characteristics very different from those of the studied cases. However, the observed phenomena and the discussed interplay between various natural periods of the system and dominant periods of the ground excitation, can be of help in predicting qualitatively the response in other cases, or in interpreting the results of numerical studies.

Acknowledgments

Financial support for this project was provided by the National Center for Earthquake Engineering Research, FHWA Contract DTFH61-92-C-00112, Task 112-D-3.7. The first author received partial funding from a Caratheodory grant from University of Patras (D.388). Thanks are also due to Mr. Peter Edinger, Partner, Mueser-Rutledge Consulting Engineers and Professor Christos Vrettos for reviewing the manuscript and offering valuable

comments, and to the staff of MRCE for preparing some of the drawings. The authors would also like to acknowledge the help of Ms. Evangelia Garini in preparing Tables 1b and 2b.

References

[1] Kramer S. Geotechnical earthquake engineering. Englewood Cliffs, NJ: Prentice-Hall; 1996.
[2] Finn WDL. State-of-the-art of geotechnical earthquake engineering practice. Soil Dyn Earthq Eng 2000;20(1–4):1–15.
[3] Stewart JP, Seed RB, Fenves GL. Seismic soil–structure interaction in buildings. II: empirical findings. J Geotech Eng ASCE 1999; 125(1):38–48.
[4] Kim S, Stewart JP. Kinematic soil–structure interaction from strong motion recordings. J Geotech Geoenv Eng ASCE 2003;129(4): 323–35.
[5] Kausel E, Roesset JM, Christian JT. Nonlinear behavior in soil–structure interaction. J Geotech Eng Div ASCE 1976;102(GT12): 1159–78.
[6] Schnabel PB, Lysmer J, Seed HB. SHAKE: a computer program for earthquake response analysis of horizontally layered sites. Report EERC 72-12, University of California, Berkeley, 1972.
[7] Roesset JM. Soil amplification of earthquakes. In: Desai CS, Christian JT, editors. Numerical methods in geotechnical engineering. New York: McGraw-Hill; 1977. p. 639–82 [chapter 19].
[8] Elsabee F, Morray JP, Roesset JM. Dynamic behavior of embedded foundations. Research Report R77-33, MIT, 1977.
[9] Newmark NM, Rosenblueth E. Fundamental of earthquake engineering. Englewood Cliffs, NJ: Prentice-Hall; 640pp.
[10] Luco JE, Westman RA. Dynamic response of circular footings. J Eng Mech Div ASCE 1971;97(EM5):1381.
[11] Elsabee F, Morray JP, Roesset JM. Dynamic behavior of embedded foundations. Research Report R77-33, MIT, 1977.
[12] Tassoulas JL. An investigation of the effect of rigid sidewalls on the response of embedded circular foundations to obliquely-incident SV and P waves. Dynamic soil–Structure Interaction. Kotterdam: A.A. Balkemal; 1984. p. 55–63.
[13] Harada T, Kubo K, Katayama T. Dynamic soil–structure interaction by continuum formulation method. Report No. 190, Institute of Industrial Science, University of Tokyo, 1981.
[14] Wolf JP. Simple physical models for foundation vibrations. Englewood Cliffs, NJ: Prentice-Hall; 1994.
[15] Gazetas G, Yegian M. Shear and Rayleigh waves in soil dynamics. ASCE 1979;105(GT12):1455–70.
[16] Gazetas G. Vibrational characteristics of soil depostis with variable wave velocity. Int J Numer Anal Meth Geomech 1982;6:1–20.
[17] O'Rourke MJ, Bloom M, Dobry R. Apparent propagation velocity of body waves. Earthq Eng Struct Dyn 1982(10):283–94.
[18] Vrettos C. In-plane vibrations of soil depostis with variable shear modulus: I. surface waves. Int J Numer Anal Meth Geomech 1990;14:209–22.
[19] Vrettos C. Dispersive SH-surface waves in soil deposits of variable shear modulus. Soil Dyn Earthq Eng 1990;9:255–64.
[20] Luco JE, Westman RA. Dynamic response of circular footings. J Eng Mech Div ASCE 1971;97(EM5):1381.
[21] Tassoulas JL. An investigation of the effect of rigid sidewalls on the response of embedded circular foundations to obliquely-incident SV and P Waves. Dynamic soil–structure interaction. Rotherdam: A.A. Balkema; 1984. p. 55–63.
[22] Harada T, Kubo K, Katayama T. Dynamic soil–structure interaction by continuoum formulation method. Report No 190, Institute of Industrial Science, University of Tokyo, 1981.
[23] Veletsos AS, Nair VV. Seismic interaction of structures on hysteretic foundations. J Struct Eng ASCE 1975;101(1):109–29.
[24] Gazetas G. Analysis of machine foundation vibrations: state of the art. Int J Soil Dyn Earthq Eng 1983;2:2–42.
[25] Gazetas G, Mylonakis G. Seismic soil–structure interaction: new evidence and emerging issues, emerging issues paper. Geotech Spec Publ ASCE 1998(75):1119–74.
[26] Richart FE, Hall JR, Woods RD. Vibrations of soils and foundations. Englewood Cliffs, NJ: Prentice-Hall; 1970.
[27] Mylonakis G, Nikolaou A, Gazetas G. Soil–pile–bridge seismic interaction: kinematic and inertial effects. Part I: soft soil. J Earthq Eng Struct Dyn 1997;26:337–59.
[28] Luco JE. Impedance functions of a rigid foundation on a layered medium. Nucl Eng Des 1974;31:204–17.
[29] Kausel E, Roesset JM. Dynamic stiffness of circular foundations. J Eng Mech Div ASCE 1975;101:771–85.
[30] Wong HL, Luco JE. Tables of impedance functions for square foundations on layered media. Soil Dyn Earthq Eng 1985;4:64–81.
[31] Dobry R, Gazetas G, Stokoe KH. II Dynamic response of arbitrarily shaped foundations: experimental verification. J Geotech Eng Div ASCE 1986;112(2):136–49.
[32] Guzina BB, Pak RYS. Vertical vibration of a circular footing on a linear-wave-velocity half-space. Geotechnique 1998;48(2):159–68.
[33] Vrettos C. Vertical and rocking impedances for rigid rectangular foundations on soils with bounded non-homogeneity. Earthq Eng Struct Dyn 1999;28:1525–40.
[34] Karabalis DL, Beskos DE. Dynamic response of 3-D rigid surface foundations by time domain boundary element method. Earthq Eng Struct Dyn 1984;12:73–93.
[35] Qian, Beskos DE. Dynamic interaction between three-dimensional rigid surface foundations and comparison with the ATC-3 provisions. Earthq Eng Struct Dyn 1995;24(3):419–37.
[36] Gazetas G. Formulas and charts for impedances of surface and embedded foundations. J Geotech Eng ASCE 1991;117(9):1363–81.
[37] Stokoe KH, Richart FE. Dynamic response of embedded machine foundations. J Geotech Eng Div ASCE 1974;100(GT-4):427–47.
[38] Novak M. Experiments with shallow and deep foundations. In: Gazetas G, Selig ET, editors. Vibration problems in geotechnical engineering. New York: ASCE; 1985. p. 1–26.
[39] Dobry R, Gazetas G. Dynamic response of arbitrary shaped foundations. J Geotech Eng Div ASCE 1986;112(2):109–35.
[40] Gazetas G, Stokoe KH. Free vibration of embedded foundations: theory versus experiment. J Geotech Eng ASCE 1991;117(9): 1382–401.
[41] Hadjian AH, Luco JE. On the importance of layering on impedance functions. In: Proceedings of the sixth world conference on earthquake engineering, New Delhi, 1977.
[42] Gazetas G, Roesset JM. Forced vibrations of strip footing in layered soils. Method Struct Anal ASCE 1976;1:115–31.
[43] Guzina BB, Pak RYS. Multi-layer representation of continuous insitu profiles in soil dynamics. Geotechnical special publication, vol. 64. New York: ASCE; 1997. p. 1–10
[44] Awojobi AO. Vertical vibration of a rigid circular foundation on Gibson soil. Geotechnique 1972;22:333–43.
[45] Awojobi AO. Torsional vibration of a rigid circular body on a non-homogeneous elastic stratum. Quart J Mech Appl Math 1973; 26:235–47.
[46] Gazetas G. Static and dynamic displacements of foundations on heterogeneous multilayered soils. Geotechnique 1980;2:159–77.
[47] Muravskii GB. Mechanics of non-homogeneous and anisotropic foundations. New York: Springer; 2001.
[48] Kassir MK, Chuaprasert MF. A rigid punch in contact with a non-homogeneous elastic solid. J Appl Mech ASME 1974;41:1019–24.
[49] Meek JW, Veletsos AS. Simple models for foundations in lateral and rocking motion, Preprints, Fifth world conference on earthquake engineering. International Association for Earthquake Engineering, Rome, 1973. 4pp.
[50] Wolf JP. To radiate or not to radiate. Earthq Eng Struct Dyn 1996;25(12):1421–32.
[51] Gazetas G. Foundation vibrations. In: Fang HY, editor. Foundation engineering handbook. 2nd ed. New York: Van Nostrand Reinholds; 1991. p. 553–93 [chapter 15].

[52] Lysmer et al. FLUSH-a computer program of approximate 3-D analysis of soil–structure interaction problems. Report No. EERC 75-30, University of California, Berkeley; 1975.
[53] Gerolymos N, Gazetas G. Constitutive model for 1–D cyclic soil behavior applied to seismic analysis of layered deposits. Soils Found 2005;45(3):147–60.
[54] Borja RI, Wu WH. Vibration of foundations on incompressible soils with no elastic region. J Geotech Eng ASCE 1994;120(9): 1570–92.
[55] Gerolymos N, Escoffier S, Gazetas G, Garnier J. Numerical modeling of cyclic lateral pile load experiments. J Geotech Geoenv Eng, submitted for publication.
[56] Gerolymos N, Gazetas G. Phenomenological model applied to inelastic response of soil–pile interaction systems. Soils Found 2005;45(4):119–32.
[57] Jakub M, Roesset JM. Nonlinear stiffness of foundations. Research Report R77-35, MIT; 1977.
[58] Tschebotarioff GP. Foundations, retaining and earth structures. 2nd ed. New York: McGraw-Hill; 1973.
[59] Mylonakis G, Nikolaou A, Gazetas G. Parametric results for seismic response of pile supported bridge bents. NCEER-95-0021, National Center for Earthquake Engineering Research, State University of New York, Buffalo, 1995.
[60] Mylonakis G, Gazetas G. Seismic soil-structure interaction: beneficial or detrimental? J Earthq Eng 2000;4(3):377–401.
[61] Mylonakis G, Gazetas G, Nikolaou S, Chancey A. Development of analysis and design procedures for spread footings. Research Report MCEER-02-0003, Multidisciplinary Center for Earthquake Engineering Research, State University of New York, Buffalo, 2002. p. 245.
[62] Gerolymos N, Gazetas G, Mylonakis G. Natural period and damping of bridge-piers on piles. In: Second international conference in geotechnical earthquake engineering, Lisbon, 1999. p. 299–96.
[63] O'Rourke MJ, Castro G, Hossain I. Horizontal soil strain due to seismic waves. J Geotech Eng ASCE 1984;110(9):1173–87.